Atmospheric Environment 293 (2023) 119449

Contents lists available at ScienceDirect

Atmospheric Environment

journal homepage: www.elsevier.com/locate/atmosenv

Integrating dual C and N isotopic approach to elemental and mathematical solutions for improving the PM source apportionment in complex urban and industrial cities: Case of Tarragona - Spain

Edson Plasencia Sánchez [a,*], Francisco Sánchez-Soberón [b,1], Joaquim Rovira [b,c], Jordi Sierra [b,d], Marta Schuhmacher [b], Albert Soler [a], Clara Torrentó [a], Mònica Rosell [a]

[a] Grup MAiMA, SGR Mineralogia Aplicada, Geoquímica i Geomicrobiologia, Department de Mineralogia, Petrologia i Geologia Aplicada, Facultat de Ciències de la Terra, Institut de Recerca de l'Aigua (IdRA), Universitat de Barcelona (UB), Martí Franquès s/n, 08028, Barcelona, Spain
[b] Environmental Analysis and Management Group, Chemical Engineering Department, Universitat Rovira i Virgili, Tarragona, Spain
[c] Laboratory of Toxicology and Environmental Health, School of Medicine, IISPV, Universitat Rovira i Virgili, Reus, Spain
[d] Laboratory of Soil Science, Faculty of Pharmacy, Universitat de Barcelona, Av. Joan XXIII s/n, 08028, Barcelona, Catalonia, Spain

HIGHLIGHTS

- PM source apportionment was assessed in a complex urban and industrial city.
- Seasonal PM_1, $PM_{2.5}$ and PM_{10} samples at the outdoor of 14 schools were collected.
- Samples were chemically, mineralogically and isotopically (C, N) characterised.
- Bayesian isotope mixing model reduced the unaccounted mass vs conventional methods.
- Long-distance and secondary particles can be uncovered by this novel approach.

GRAPHICAL ABSTRACT

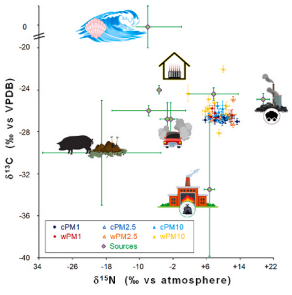

ARTICLE INFO

Keywords:
PM10
PM2.5
PM1
Stable isotopes
Mixing models
Tarragona

ABSTRACT

Identification of dominant airborne Particulate Matter (PM) sources is essential for maintaining high air quality standards and thus ensuring a good public health. In this study, different approaches were applied for source apportionment of three PM fractions (PM_1, $PM_{2.5}$ and PM_{10}) at the outdoor of 14 schools of a coastal city with a significant land use interweaving such as Tarragona (Spain). PM were collected in 24h-quartz microfiber filters in two seasonal campaigns (cold and warm), together with nine local potential sources, so a total of 84 samples were chemically, mineralogically, and isotopically characterised. Source apportionment was assessed by (i) main chemical components, (ii) Principal Component Analysis (PCA), (iii) dual C and N isotope approach, and (iv) a Bayesian isotope mixing model. When chemical concentrations were grouped into marine, crustal, secondary inorganic aerosols and organic matter + elemental carbon categories, the unaccounted component reached 45% of PM mass. The PCA allowed to identify also traffic and industrial contributions, reducing the unaccounted mass to about 25%. Adding $\delta^{13}C$ and $\delta^{15}N$ values, secondary organic aerosol could be estimated and a continuous contribution of diesel combustion was identified together with a remarkable use of natural gas in winter. Isotopic

* Corresponding author.
E-mail address: eplasencia@ub.edu (E. Plasencia Sánchez).
[1] Present address: Institute of Health Carlos III, Department of Atmospheric Pollution, 28220 Madrid, Spain.

https://doi.org/10.1016/j.atmosenv.2022.119449
Received 31 May 2022; Received in revised form 8 October 2022; Accepted 24 October 2022
Available online 29 October 2022

values were better understood when considering air masses back trajectories and a possible long-distance contribution from coal-fired electric generating units (EGUs). Finally, using Bayesian dual isotope mixing models, the unaccounted PM mass was reduced up to 5% when adding these EGUs to marine-carbonate related, road traffic, domestic heating, waste incinerator and livestock waste contributions. The added value of the dual isotope approach combined with a Bayesian isotope mixing model, in comparison with conventional chemical approaches, was thus demonstrated for PM source apportionment in an urban and industrial site where many sources and processes converge and can then be applied to other complex cities.

1. Introduction

Particulate Matter (PM) is any mixture of airborne solid particles and liquid droplets, including sea spray, soot, pollen, fly ashes, metals, acids, and hundreds of inorganic and organic species directly released or formed as secondary aerosols after complex reactions in the atmosphere (US Environmental Protection Agency, 1996; Fan and Lin, 2011). A close relationship between high PM levels and adverse effects on health has been reported in several epidemiological studies (Davidson et al., 2005; Salvi, 2007; Olmo et al., 2011). Most of these studies have focused on coarse particles (PM_{10}) and fine particles ($PM_{2.5}$), although there are evidences on the adverse effects of the inhalation of submicron particles (PM_1) on lung tissues and alveolar cells (Ferin et al., 1992; Yeh et al., 1997; Sánchez-Soberón et al., 2018).

Identification of dominant PM sources is essential for the formulation of future control policies and for the development of pollution mitigation strategies to protect public health (EC – European Council, 2008). Traditionally, most PM source apportionment studies are focused on a deterministic identification of the sources and the quantification of their relative contribution (Querol et al., 2001; Amato et al., 2016). To these ends, PM chemical profiles are linked with specific air pollution sources according to for example: (i) chemical affinity (Querol et al., 2004a); (ii) statistical correlation (Alastuey et al., 2007) or (iii) using selected trace element ratios (Mbengue et al., 2017). In this way, some of the identified emission sources include road traffic, coal and heavy fuel combustion, oil refineries, ceramic industries, ferromanganese industry, non-exhaust traffic and fireworks (Moreno et al., 2013). If all sources' chemical profiles are well known, a Chemical Mass Balance (CMB) can then be performed directly to obtain the contributions from each source to the total PM mass (Friedlander, 1973). Otherwise, a Factor Analysis (FA) technique needs to be applied for solving the receptor model (Watson et al., 2002). Principal Component Analysis (PCA) is one of the most widely used technique, since it consumes less computational time (Jakeman et al., 2008) and allows to scale the data easily (Tauler et al., 2009).

The use of stable isotopes has emerged as a useful tool for identifying PM emission sources (Aguilera and Whigham, 2018; Widory, 2007). Using isotopes of only one element can present some limitations to distinguish among different sources in complex systems, and this is why multiple element isotope studies are preferable. The application of multi-element isotopic approaches is however still scarce for PM sources identification (e.g. Widory et al., 2004a; Souto-Oliveira et al., 2018). Specifically, a dual isotopic approach combining $\delta^{13}C$ of total C and $\delta^{15}N$ of total N in PM has been barely used for identifying PM sources (Kunwar et al., 2016; Morera-Gómez et al., 2018; Lim et al., 2019), and these studies have mainly focused on PM_{10} and/or $PM_{2.5}$, excluding PM_1 particles. In large cities or in locations where one or two emission sources are predominant, isotopic analysis can be complemented by air masses back trajectories analysis (Wakamatsu et al., 1996; Sharma et al., 2015; Souto-Oliveira et al., 2018).

Once the sources are identified, their proportional contribution to the mixture can be quantified based on their stable isotopic signatures by a deterministic analytical solution, the end-member mixing method (EMM) or by other improved probabilistic approaches including Bayesian statistical concept (Phillips and Gregg, 2003; Parnell et al., 2013). Bayesian isotope mixing models have been rarely applied to PM source apportionment (Wang et al., 2017; Li et al., 2020) and to our knowledge, never using the dual isotope (C and N) approach.

The objective of this study is thus to assess the added value of the dual isotope approach combined with an isotope mixing model, in comparison with chemical approaches, for PM source apportionment in complex urban and industrial sites where many sources converge. Tarragona (Catalonia, NE Spain) was used as a model city. It has been considered as one of the most industrialised zones in southern Europe (Domínguez-Morueco et al., 2017). Indeed, the chemical industry of the province of Tarragona represents 12% of the Spanish industrial Gross Domestic Production (AEQT, 2019). The Tarragona province, with a total population of around 800 thousand people (INE, 2019), is affected by intense road traffic (registered fleet of 24 thousand of vehicles, DGT, 2020) and tourism demand (50 million of overnights per year, GENCAT, 2022). Agriculture and cattle industry are also very significant in Catalonia, accounting for about 40% of national swine industry, 50% of swine processing activities and 56% of the exported pork products volume (MAPA, 2020). Previous works have addressed PM sources apportionment in this city, mainly using chemical receptor models (Viana, 2003; Moreno et al., 2006; Alastuey et al., 2007). Most of these studies are focused in PM_{10} and/or $PM_{2.5}$, whereas PM_1 have not yet been studied in Tarragona.

Since children are one of the population groups more vulnerable to particle exposure, due to their greater inhalation rate per body weight and their developing immune system (Liu et al., 2018; Thurston, 2000), we focused on PM from the outdoor of schools. Three PM fraction levels (PM_1, $PM_{2.5}$ and PM_{10}) were sampled in the outdoor of 14 schools together with 9 potential local PM sources at Tarragona with the aim of proposing a dual-isotope mixing model as a tool to improve the PM source apportionment. To this end, chemical and ionic profile together with C and N stable isotopic composition were determined and the sources contribution was assessed by different approaches, including main chemical components, CMB and PCA, by exploring the relationship between Total Nitrogen (TN) and $\delta^{15}N$ and between Total Carbon (TC) and $\delta^{13}C$, by loading the back trajectories for the corresponding air masses (through US NOAA HYSPLIT model), and by evaluating a dual C and N isotope approach with a Bayesian isotope mixing model.

2. Methodology

2.1. Site description and sampling campaigns

The city of Tarragona is located in northeast Spain on the shore of the Mediterranean Sea at 90 km southwest of Barcelona. Four industrial estates are located in the vicinity of the city. The North Complex (or Petrochemical area) includes an oil refinery and several petrochemical industries. The South Complex includes several chemical plants and is located close to an important industrial harbour. The Constantí industrial estate contains a Hazardous Waste Incinerator (HWI) at the northwest. The Riu Clar estate contains a Municipal Solid Waste Incinerator (MSWI) at the southeast (Fig. 1). Fourteen schools were selected to assess outdoor air quality in two seasonal sampling campaigns (cold and warm). The selected schools (see ID number in Fig. 1) are distributed around the different industrial estates. In addition, a school located in another coastal town, Cambrils, 6 km away from any industrial estate, was selected as background (ID1 in Fig. 1).

At each school and only during school days, three PM fractions (PM_1, $PM_{2.5}$ and PM_{10}) were collected using high-volume active samplers: CAV-A/mb (MCV SA) for PM_1 and TE-6070-DV (Tisch Environmental) for $PM_{2.5}$ and PM_{10}. The air volume sampled after 24 h was around 600 m^3 for PM_1 and 1700 m^3 for $PM_{2.5}$ and PM_{10} (see Supporting Information, S.I. Table A1 for checking specific sampling dates). Prior to each sampling campaign, the quartz microFiber Filters (QFFs) used for PM sampling were heated at 200 °C for 4 h, stabilized at 40% Relative Humidity (RH) and 25 °C and then weighted similar to other studies (Sanchez-Soberón et al., 2015; Rovira et al., 2018; Millán-Martínez et al., 2021). After sampling, the QFFs were wrapped separately with aluminium foil and stabilized under the same previous conditions of temperature and humidity to elucidate PM mass by weight difference (please check S.I. A.1.2 for final PM estimation). Once the gravimetric determination was performed, QFFs were stored in a freezer at −60 °C until further analysis. Blank field filters were treated in the same way as the rest of the QFFs.

In the cold campaign (December 2016 to March 2017), twelve schools were sampled (ID1-12). During the warm campaign (September to October 2017), one school (ID5) was replaced by the nearest one (ID13) due to logistic considerations, and an additional school (ID14) was included and considered as a second background location to have both inland and coastal background references. As a result, a total of 25 samples were obtained for each PM fraction. All the outdoor PM samples were collected at the same time that indoor counterpart samples in the framework of a project assessing children's exposure to PM (Sánchez-Soberón et al., 2019).

The mean average temperatures were 10.7 °C for the cold campaign and 21.6 °C during the warm campaign. Predominant winds blew alternatively in both ways of the north-south direction regardless of season due to the influence of the Mediterranean Sea. Average wind speed was 8.4 km/h and 7.6 km/h during the cold and the warm campaign, respectively (Sánchez-Soberón et al., 2019).

To consider potential local PM sources, we tried to obtain representative samples of industrial complexes emissions through their business association, *Associació Empresarial Química de Tarragona* (AEQT). However, we only got six samples without much information about how, when or where they were collected (S.I. Table A2). Attending to their visual aspect, one sample was labelled as domestic burned firewood (M5) and another was supposed to come from the MSWI (M3), but the other four were completely blind samples (M2, M7-M9). Additionally, three more samples from other potential local PM sources were collected; one was collected from granulated carbon laying on the industrial harbour (M4) and two soot samples were obtained by rubbing directly with a QFF the inside surface at the end of a gasoline and diesel car tailpipe, respectively (M6 and M1).

2.2. Analytical methods and quality assurance

Concentration of major and trace elements and soluble ions, listed in S.I. A.1.2, was determined following the methodology described by Rovira et al. (2018). In brief, an average of 30 mg for samples in powder or a quarter of QFF was acid digested with a mixture of 2 mL of nitric acid (65% V/V, Merck) and 3 mL of hydrofluoric acid (37.5% V/V, Panreac) in a Teflon vessel for 8 h at room temperature followed by 8 h at 80 °C. The digested solution was evaporated until dryness on a sand bath at 250 °C. The residue was re-dissolved in 2.5 mL of nitric acid and diluted to a final volume of 25 mL with ultrapure water. This solution was kept at −20 °C until further analysis by Inductively Coupled Plasma Optical Emission Spectrometry (ICP-OES, PerkinElmer Optima 3200RL) for major elements and by Inductively Coupled Plasma Mass Spectrometry (ICP-MS, PerkinElmer Elan 6000) for trace elements. Another 30 mg or another quarter of each QFF was cut in smaller pieces and water leached with 15 mL of deionised water in a Falcon tube during 4 h, followed by sonication at 60 °C during 1 h. The extract was 0.22-μm filtered and analysed by Ionic Chromatography (IC, DX-300 Dionex) for determining the ionic content (i.e., chlorides, nitrates and sulphates) and by spectrophotometry using Berthelot's reagent for ammonium. From 1 cm^2 of the third QFF quarter approximately or 10 mg of powder, the total carbon (TC), nitrogen (TN) and sulphur (TS) content was determined by combustion in presence of oxygen at 1000 °C. The generated gases (CO_2, NO_2 and SO_2) were driven by a helium flow and analysed by using an Elemental Analyser (EA, EA 1108 CHNS–O Carlo Erba, Thermo).

All the chemical analyses were performed in duplicate and the blank field filters were analysed under the same conditions as real samples.

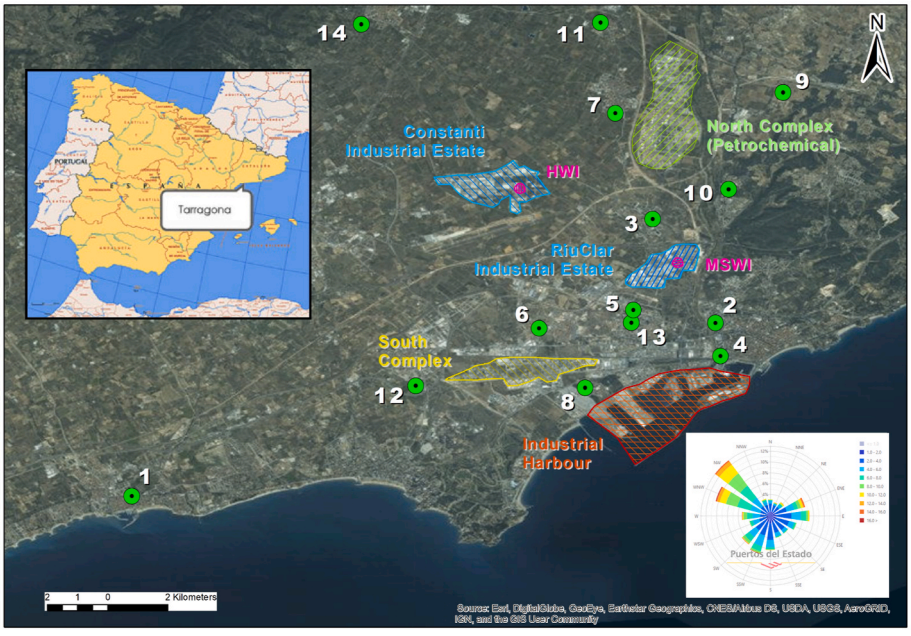

Fig. 1. Location and ID number of the 14 schools sampled in this study together with the location of most relevant industrial clusters. The 2016–2017 multi-annual wind rose at Tarragona harbour (Puertos del Estado, 2021) is also shown. The base map (World Imagery – Clarity) was obtained from ArcGIS10.2.

Following Sánchez-Soberón et al. (2019), concentrations in the samples were calculated as the difference between the average of their duplicates for each sample and their mean concentration in the blank field filters. Environmental (outdoor) air concentrations (μg/m^3) for QFFs were obtained by considering the proportional air sampled volume to the used QFF area in each analyse as a multiplicative factor for each mass concentration. A full list of analysed elements, limits of detection (LoD) and further details of Quality Control/Quality Assurance (QC/QA) procedures can be found in S.I. A.1.2.

Mineralogical and isotopic characterisation of the samples was carried out at the *Centres Científics i Tecnològics de la Universitat de Barcelona* (CCiT-UB). The mineralogy and morphology of individual particles from the samples of potential local PM sources and the QFFs from the cold campaign were analysed by X-Ray Diffraction (XRD) and Scanning Electron Microscopy with Energy-Dispersive X-ray Spectroscopy (SEM-EDS), respectively. Methodological details can be found in S.I. A.1.3.

Bulk carbon and nitrogen stable isotopic compositions for all samples including the potential local PM sources, blanks and QFFs from both cold and warm campaigns were analysed by an EA (Carlo Erba Flash 1112) coupled to an Isotope Ratio Mass Spectrometer, IRMS (Delta C, Thermo) through the interface Conflo III (EA-IRMS). Powder samples (M2-M5) were directly weighted in tin capsules (8 × 5 mm), while for QFF samples (n = 80) small pieces of approximately 10 × 10 mm were cut and compacted inside the capsules. Isotope data are expressed using the conventional delta notation (δ) in ‰ relative to the Vienna Pee Dee Belemnite (VPDB) and atmospheric N_2 standards for carbon and nitrogen, respectively:

$$\delta^{13}C \text{ and } \delta^{15}N = \left(\frac{R_{sample} - R_{standard}}{R_{standard}}\right) x1000$$

As part of QA/QC scheme, δ^{13}C of TC and δ^{15}N of TN were obtained based on two-point normalization using international reference materials: USGS 40, IAEA CH6 and IAEA CH7 for C, and USGS 40, IAEA N1 and IAEA N2 for N, according to Coplen et al. (2006). These reference materials were interleaved among samples along the analysis period, their typical errors were below 0.3‰ for carbon and 0.5‰ for nitrogen (n = 34). Isotopic signals (*m/z* 44 and 28 respectively for C and N) below 250 mV in EA-IRMS were not considered valid results. Forty-eight (out of 75) δ^{13}C and 37 (out of 75) δ^{15}N reliable values were obtained from the filters using this method. Nevertheless, IRMS signal for the remaining samples was too low even by using a He dilution pressure of 0.5 bar or increasing the mass of filter inside the capsule. An alternative method consisting in scraping small pieces of QFFs off into the tin capsules and turning the He dilution off resulted in reliable δ values for most of the remaining samples. A subset of samples was used for developing and validating a linear regression model for δ values from scraping method to the corresponding TC and TN content (see S.I. A.1.4 for more details).

As a result of both methods, a total of 75 δ^{13}C and 51 δ^{15}N values were obtained for the three PM fractions. For those samples in which pieces of filters were directly packed into the capsules, the measurement uncertainty was considered as standard deviation from measurements of reference materials along the analysing period (values stated above). For those samples for which the scraping method was used, analytical uncertainty was set to the maximum Mean Squared Error (MSE) of the corresponding normalizing linear model, which means ± 0.6‰ for carbon and ±1.4‰ for nitrogen. δ values for blank filters were equals to those obtained for empty tin caps for carbon (−27.5‰) and below LoD for nitrogen.

2.3. Data analysis

The Limit of Quantitation (LoQ) was computed for the whole dataset according to Wenzl et al. (2016) and Mocak et al. (1997). Only values above the LoQ were used, plotted and analysed, except when it was needed to perform numerical operations over the whole data, in which case, a half of maximum available value (the maximum value of the replicas) was assigned instead of a half of LoQ in order to avoid biases (Ahn et al., 2008). Contents of aluminium oxide (Al_2O_3) and silicates (SiO_2) in PM were indirectly determined from the contents of Al, as previously done by Alastuey et al. (2007) and Pey (2008), i.e., 1.89 × Al = Al_2O_3 and 3 × Al_2O_3 = SiO_2. The levels of Organic Carbon plus Elemental Carbon (OC + EC) were obtained by subtracting the concentration of C in carbonates (C–CO_3^{2-} = Ca + Mg – SO_4^{2-}) from the TC. The marine sulphate (marine SO_4^{2-}) was indirectly determined by stoichiometry from the soluble Na levels (marine SO_4^{2-} = Na^+ × 0.25) in accordance to the Na^+/SO_4^{2-} sea water ratio (8.33 Na^- eq/Cl^- eq, Drever, 1982). The remaining sulphate was considered nonmarine sulphate. Secondary Inorganic Aerosols (SIA) result from the sum of nonmarine sulphate, nitrate and ammonium (nonmarine SO_4^{2-} + NO_3^- + NH_4^+). Organic Matter plus Elemental Carbon (OM + EC) was calculated by applying a 1.2 factor to the OC + EC concentration as done before for Tarragona studies (Alastuey et al., 2007; Sánchez-Soberón et al., 2019). Due to its presence in the QFF matrix, Ba was not considered at any stage. The Total Metal (TM) content was calculated as the sum of metal and metalloid elements.

A CMB was tested as a first attempt for estimating contributions from the obtained potential local sources (see S.I. A.2.5.). However, the variability found in these sources did not match properly the one in the QFFs samples, making their contribution negligible. This fact reinforced our idea that sampled potential local PM sources were not representative enough of air pollution sources for the studied schools. We considered that additional samples from other potential local PM sources would be needed if further source apportionment studies were conducted using this method.

Then, a PM mass distribution was performed based on the four major chemical components, following the chemical receptor model of Querol et al. (2004a). Furthermore, a special dataset of the whole chemical database was prepared (major and trace elements concentrations were expressed in μg/m^3 and ng/m^3, respectively) following Tauler et al. (2009) and was analysed by PCA, for identifying potential sources according to QFFs chemical composition using Statgraphics XVII. Kaiser-Meyer-Olkin (KMO) factorability test and Bartlett's sphericity test (BST) were performed to examine the validity of PCA (see S.I. A.2.9.).

Identification of potential sources based on isotope data was performed by comparison between the obtained isotope dataset and literature δ^{13}C and δ^{15}N values for PM sources that could be relevant for the city of Tarragona. Nine potentially relevant atmospheric emission sources were considered. Table 1 summarizes their δ^{13}C and δ^{15}N values collected from the literature. S1 and S2 stand for particles generated from combustion gases released by road traffic. S3 corresponds to the particles generated from combustion gases released by coal-fired EGUs (Felix et al., 2012). S4 represents marine aerosols, which could represent an important emission source for a coastal location. S5 represents the contribution of livestock industry and the common use of pig manure as fertilizer in Catalonia (Puig et al., 2013) to the airborne PM through both transport process of dry waste and the nucleation and deposition processes of their emitted gases. With minimum temperature lower than 10 °C in winter (GENCAT, 2020), the use of domestic heating units (S6, S7 and S8) is highly expected in the area; nevertheless, there is no available information about the most used fuel. One can presume that natural gas is the preferred fuel by the amount of residential installations, nevertheless, recent reports indicate an increase in the use of wood (pellets and others) as fuel for heating in Catalonia (GENCAT, 2019b; Querol et al., 2016). S9 considers the proximity to the MSWI at Riu Clar estate.

For a further source apportionment analysis based on dual isotope data, a Bayesian isotope mixing model was used to estimate the proportional contributions of selected sources (S1 to S9 in Table 1) to bulk C and N in the PM fractions. The MixSIAR (Stock et al., 2018) model

Table 1
Mean $\delta^{13}C$ and $\delta^{15}N$ (± standard deviation, SD) values reported for selected atmospheric emission sources.

Source (ID-Description)	$\delta^{13}C$ (‰)	n	references	$\delta^{15}N$ (‰)	n	references
S1 – Vehicle exhaust-NO_x related	−26.8 (1.6)	5	[a, b]	−2.5 (1.5)	78	[c]
S2 – Vehicle exhaust-NH_3 related	−26.8 (1.6)	5	[a, b]	−3.4 (1.7)	2	[d]
S3 – Coal-fired EGU	−24.9 (0.6)	95	[e]	+19.5 (1.4)	16	[f]
S4 – Marine aerosol-carbonate related	0.0 (2.0)	20	[g]	−8.0 (8.0)	8	[d, h]
S5 – Livestock waste	−24.0 (5.1)	12	[d, i]	−19.0 (14.1)	15	[d, j, k, l]
S6 – Coal-heating exhaust	−24.0 (0.4)	8	[a]	−5.3 (0.5)	1	[m]
S7 – Fuel-oil-heating exhaust	−26.9 (0.5)	5	[a]	−7.7 (8.8)	8	[m]
S8 – Natural gas-heating exhaust	−24.4 (0.6)	4	[a]	+7.9 (5.9)	5	m
S9 – Waste incinerator (MSWI)	−33.5 (6.4)	2	[n]	+6.7 (1.3)	2	n

$\delta^{15}N$ values for S1 were obtained from modelling 78 experimental values. Only δ values for EGU with Selective Catalytic Reduction (SCR) technology were considered in S3. δ values for S5 include those reported up to 2.5 cm depth in carbonates of livestock corrals. Isotopic values for coal-fired waste incinerator were excluded in S9.

[a] Widory et al. (2004a).
[b] López-Veneroni (2009).
[c] Walters et al. (2015).
[d] Felix et al. (2013).
[e] Suto and Kawashima (2016).
[f] Felix et al. (2012).
[g] Bornemann et al. (2012).
[h] Altieri et al. (2013).
[i] Macharia et al. (2012).
[j] Freyer (1978).
[k] Heaton (1987).
[l] Felix and Elliott (2014).
[m] Widory (2007).
[n] Widory et al. (2004b).

framework was used due to its friendly and customizable set of mixing model parameterization. Calibration coefficients were initialized by default, while PM size and campaign were included as categories that produce fixed effects.

To determine the origin of air masses and the possible PM transport pathways from potential sources, air back-trajectories were computed by means of NOAA Hybrid Single-Particle Lagrangian Integrated Trajectories (HYSPLIT) model (Draxler and Rolph, 2003). 24h backward trajectories were calculated at 10:00 UTC on every sampling day at 250 and 500m above the ground level at 6h intervals from Tarragona (41.1°N 1.2°E).

All statistical analyses were performed using Statgraphics XVII. The dataset was categorised by PM size and campaign. Dataset normality was evaluated by using Shapiro-Wilk's test with a significance level $\alpha = 0.05$. Mann Whitney *U* test or Welch's *t*-test and one-way Analysis of Variance (ANOVA) were applied according to the normal o non-normal distribution of the data, respectively. All maps were generated by using ArcGIS 10.2. Spatial Statistics and Spatial Analyst toolbox were used for assessing a spatial characterisation; Standard Deviational Ellipse (SDE, Yuill, 1971) for dispersion and directional distribution, and Inverse Distance Weighting interpolation (IDW, Shepard, 1968) for the most probably radius or area of influence.

3. Results and discussion

3.1. PM pollution levels

Obtained daily levels for the three PM sizes, shown in S.I. Figure A6, are consistent with daily and monthly and annual mean values previously reported for Tarragona city (Viana, 2003; Viana et al., 2006a; Alastuey et al., 2007; GENCAT, 2019a). All except one of the PM samples showed concentrations below to their corresponding 24h European air quality limits (50 and 25 μg/m^3 for PM_{10} and $PM_{2.5}$ respectively, EC – European Council, 2008). Nevertheless, more samples were above the recently updated WHO 24h air quality guideline (AQG) levels (45 and 15 μg/m^3 for PM_{10} and $PM_{2.5}$, respectively) (WHO, 2021) associated with important risks to public health based on the last scientific evidences. Although these WHO guidelines are not legally binding standards and can be exceeded 3–4 days per year, 75% of our $PM_{2.5}$ samples in the cold campaign were exceeding them which is quite noteworthy (see S.I. Figure A6). PM_1 monitoring is not yet foreseen by existing EU/WHO air quality standards, and thus there are no thresholds to compare with.

PM levels were mainly higher for the cold than for the warm campaign (S.I. Figure A6). The overall maximum values for the three PM sizes were observed at schools ID11 for the cold campaign, and ID7 for the warm campaign. These two schools, located to the west of the Petrochemical complex (Fig. 1), showed also the highest PM_{10} indoor levels for the same cold campaign (Sánchez-Soberón et al., 2019). Nevertheless, a significant correlation was not found between outdoor and indoor PM levels (data not show), likely due to the differential use of air conditioning (as filtration of coarse PM) in some schools, mainly during the warm campaign (Sánchez-Soberón et al., 2019). The lowest outdoor PM mass concentrations were registered during the warm campaign at ID1, ID6 and ID8.

Regarding PM mass size distribution, PM_1 fraction represents most $PM_{2.5}$ content for schools ID5, ID6, ID7 and ID12 ($PM_1/PM_{2.5}$ ratios of 0.76, 0.90, 1.17 and 0.62, respectively). The spatial distribution analysis reveals that the main distribution of $PM_1/PM_{2.5}$, PM_1/PM_{10} and $PM_{2.5}/PM_{10}$ ratios is along a line parallel to the shoreline (i.e., major axis of the corresponding weighted standard deviation ellipse) for both campaigns (S.I. Figure A7). The eccentricity of the ellipses is significantly different ($p = 0.10$) between warm and cold campaign (0.58 ± 0.04 and 0.65 ± 0.04, respectively), indicating different spatial distribution even though predominant wind direction remains on NW direction. Thus, the PM spatial distribution seems to be more influenced by the effective wind speed than by the predominant wind direction, showing the overlap of two effects: daily air transport from sea to land and seasonal variations in air fluxes along the coastline.

3.2. Elemental composition

The content of 55 chemical elements was analysed for each sample. Only 11% of the potential dataset resulted with values above its respective LoQ. For major elements, available data represent up to 23% of the expected, while only 8% is available for describing trace elements composition. A statistical overview of the results is summarised in S.I. Table A4. Some elements (e.g., C, Na, Ti, Cu) are prevalent (Fig. 2), but in a wide range of concentrations, evidenced by their interquartile range (IQR).

3.3. Total carbon (TC) and nitrogen (TN)

For all campaigns and PM sizes, TC ranged from 0.3 to 10.7 μg/m^3 with a mean value of 2.7 μg/m^3 ($p = 0.77$, Welch's *t*-test). The cold campaign showed a higher Coefficient of Variation (CV) (0.95–1.11) than the warm campaign (0.25–0.57). TN ranged from 0.1 to 1.8 μg/m^3 with a mean value in the warm campaign (0.70 μg/m^3) twice higher than in the cold campaign ($p < 0.05$, Welch's *t*-test). The warm

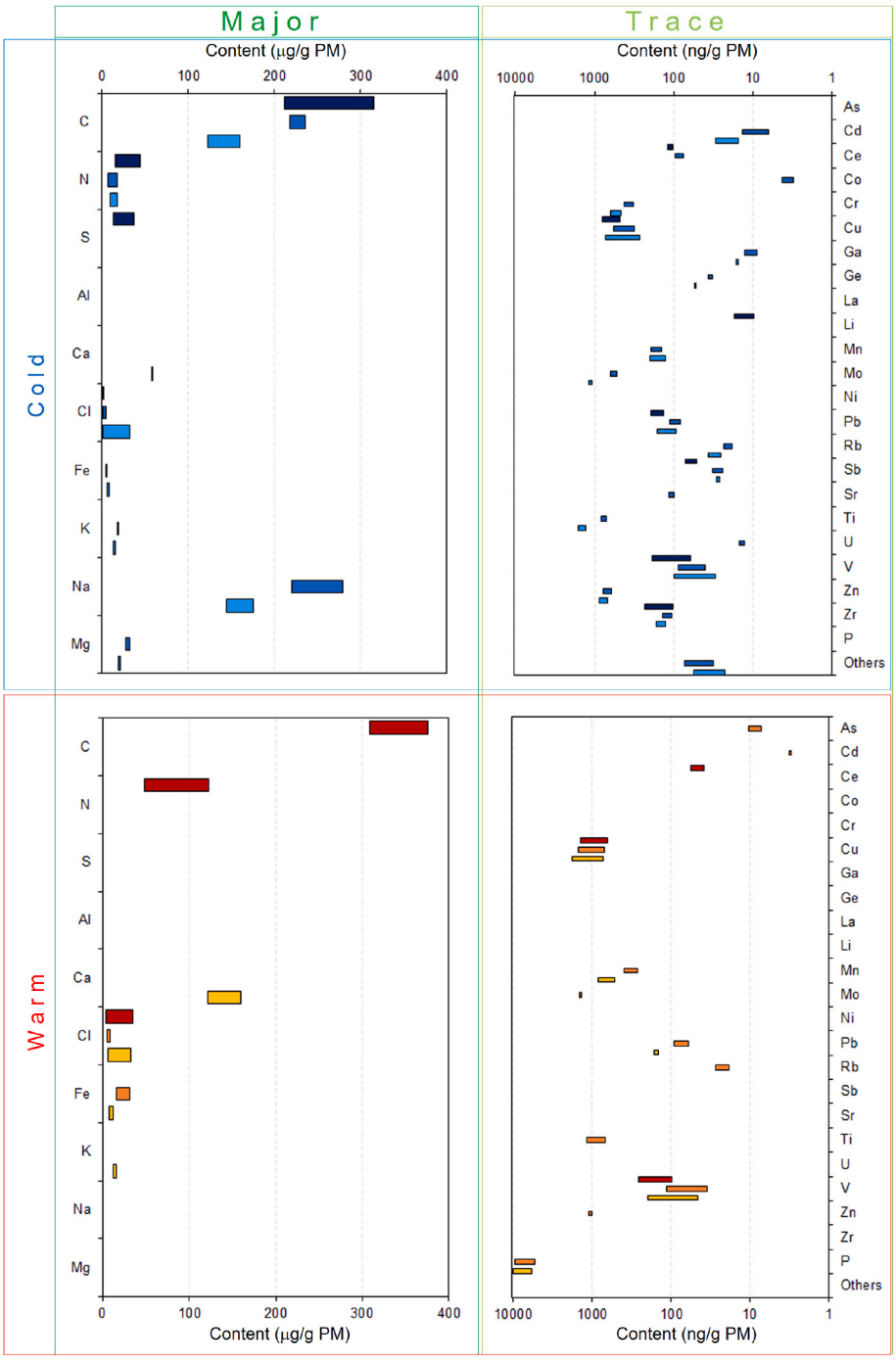

Fig. 2. Major (left panels) and trace elements (right panels) content in the 14 outdoor PM samples from schools in Tarragona, expressed through the IQR respect to PM concentrations by weight. Darkest to lightest bluish and reddish bars stand for PM_1, $PM_{2.5}$ and PM_{10} in cold (upper panels) and warm (lower panels) campaigns, respectively. Values under LoQ are not shown.

campaign presented higher variability (CV = 0.56–0.81) than the cold campaign (0.27–0.55). C and N variability can be seen graphically in Fig. 2, where values below LoQ are not represented.

The TC/TN ratio can be used to assess the origin of the organic matter (Fig. 3a), because terrestrial C4 and C3 plants have higher values than marine phytoplankton (>30, >15 and ~7, respectively) (Ertel and Hedges, 1985; Meyers, 1994). A terrestrial origin could be inferred for schools ID7 (PM_{10} cold campaign) and ID6 ($PM_{2.5}$ cold campaign). Indeed, their values (33 and 30, respectively) were similar to the maximum found for biomass burning in agriculture (8–32, Agnihotri et al., 2011). Most TC/TN values from PM_1 samples fell on the contrary within the range for marine origin, between phytoplankton (6.6, Redfield, 1958) and deep sea marine aerosol (1.9–2.9, Miyazaki et al., 2010). TC/TN values should also be interpreted as resulting from direct or indirect release of droplets from fuel combustion and their accumulation in PM emission (Wang et al., 2017; Querol and Amato, 2017) from road traffic, heating or industrial stacks, and thus, reflecting their original fuel value: petroleum or petroleum derived lubricants (prehistoric zooplankton and algae), diesel, gasoline, natural gas, biodiesel (enriched in C3-plants), coal (enriched in C4-plants) or firewood. Potential local PM sources (M1-M9) contain up to 90% of carbon, whereas only M4, M6 and M8-9 contain enough nitrogen to be plotted together

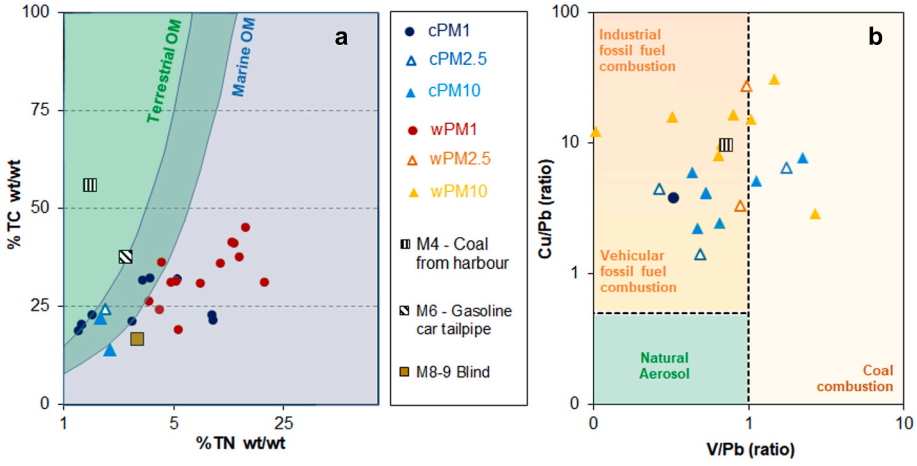

Fig. 3. (a) Origin of Organic Matter (OM) content based on TC/TN values reported by Ertel and Hedges (1985), Miyazaki et al. (2010) and Agnihotri et al. (2011) for marine phytoplankton and aerosols (Marine OM) and for coastal marine sediments and aerosols collected from burning crop residues (Terrestrial OM); (b) Origin of metal content according to Sen et al. (2016). Bluish and reddish symbols stand for cold (c) and warm (w) campaigns, respectively. The results for the potential PM local sources are also shown (when possible). Since chemical composition of M8 and M9 was quite similar, both samples are treated as the same source (M8-9) hereafter.

with school samples. M6 and M8-9 locations in Fig. 3a suggest that they could contain fuel and/or lubricant droplets.

3.4. Major and trace elements

In general, relative major and trace element content were similar in PM_{10} and $PM_{2.5}$ samples, while trace element content of PM_1 samples was significantly different among schools in the cold campaign (S.I. Table A4 and Table A5). As expected from a coastal city, Na was the most abundant element (as weight percent) in cold PM_{10} and $PM_{2.5}$ samples (17 ± 3% and 24 ± 6%). Relative content of other typical major elements as Ca and Mg levels in the PM_{10} and $PM_{2.5}$ outdoor samples were in general higher than in their counterpart indoor samples, concluding Sánchez-Soberón et al. (2019) that the outdoor mineral dust was the main source of these elements in the classrooms. The presence of mineral dust was corroborated by the identification by XRD of crystalline phases of salt (halite, NaCl) and calcite ($CaCO_3$) in coarse fraction (PM_{10}) of cold campaign samples (see example in S.I. Figure A9g). In fine ($PM_{2.5}$) and submicron (PM_1) fractions, XRD peaks of mineral phases were not so representative. By using SEM-EDS, 10 μm-sized salt crystals were frequently detected (PM_{10}, see S.I. Figure A9a), and pollen grains (S.I. Figure A9b) and clay minerals crystals (<5 μm-sized) were eventually observed ($PM_{2.5}$). In most PM_1 samples, particles enriched on Pb, Fe and Cu (<1 μm-sized) and fresh soot aggregates were identified (see S.I.Figure A9f). Soot aggregates and particles rich in Cu and Mn were previously shown in PM samples from oil/gas plants or sites influenced by road traffic/brake systems (Viana et al., 2008; Calvello et al., 2017; Di Palma et al., 2018).

A similar TM content was measured in PM_{10} and $PM_{2.5}$ samples, representing up to 30% of their PM mass. For PM_1, however, TM represents less than 1% of PM_1 mass (S.I.Table A4). There is not a clear relationship between TM and PM levels (Pearson's correlation coefficient, $0 \leq r \leq 0.55$, data not show). A k-means clustering analysis pointed to a stronger correlation at PM concentration below 20 $\mu g/m^3$ ($r = 0.60$) and at TM content lower than 3% ($r = 0.75$). Two main conclusions can be drawn from the spatial distribution of TM/PM ratios for each PM size fraction (S.I. Figure A8): the TM content decreases from the coast to the mainland (as observed for PM_{10} in the cold campaign, $r = 0.51$) and that particle nucleation mainly occurs around the industrial states (as observed for $PM_{2.5}$ in the warm campaign, $r = 0.38$).

Regarding the non-metal elements, Cl^- and P were the most abundant elements for PM_{10} and $PM_{2.5}$ samples and S was for PM_1. These facts point to sources such as marine aerosol, polychlorinated biphenyls (PCBs), organochlorine pesticides or fertilizers (Mari et al., 2009; Domingo et al., 2017; Domínguez Morueco, 2018; Maceira et al., 2018).

Other specific element content such as Mn (characteristic for metallurgical plants and steelworks), Se (usually used to identify coal combustion) and Ni (present around refining and fuel-oil combustion plants) together with some element mass ratios (S.I. Table A7) were selected as tracers for identifying PM sources in our QFFs and potential local sources samples, based on a comparative analysis among reviews (Morawska and Zhang, 2002; Viana et al., 2008) and recent studies for highly industrialised and coastal areas (Mbengue et al., 2014, 2017; Sen et al., 2016; Alves et al., 2018; Di Palma et al., 2018; Leng et al., 2018). Most remarkable findings in each of the 14 schools are summarised in S. I. Table A5. But in general, obtained values for Cu/(Zn + Pb) ratio are significantly higher than any of the geogenic sources considered by Weng et al. (2003), Volkov et al. (2017) or GGICAS (1981), although similar to those reported by Kabala and Singh (2001) for top soils in the vicinity of a copper smelter. The values for Cu/Pb ratio correspond to industrial sites (Sen et al., 2016), likely more influenced by road traffic than by MSWI or coal burning industries (Font et al., 2015; Sen et al., 2016) attending to V/Pb and Cd/Pb ratios (Fig. 3b). Obtained values for Cu/Sb ratio are significantly lower than upper Earth crust (Taylor and McLennan, 1985), but greater than those found for urban road traffic (Lin et al., 2005; Muránszky et al., 2011), suggesting that all schools are influenced by oil processing industry (Mbengue et al., 2017). The highest Cu/Sb values occurred in cold campaign at locations ID4 for $PM_{2.5}$ and ID11 for both PM_{10} and PM_1, which were slightly higher than the highest value found in the literature for PM_{10} resuspended from road dust (Alves et al., 2018). Although they could only be evaluated for cold campaign samples, Fe/Cu ratio pointed also to emissions from road traffic according (Iijima et al., 2007; Hulskotte et al., 2014), and Cl/Na ratio values were much lower than those expected for marine salt, but similar to those found for Tarragona's harbour (Alastuey et al., 2007). This could be due to the well-known reaction between ammonium nitrate (NH_4NO_3) and salt (NaCl) that takes place when PM_{10} and $PM_{2.5}$ are sampled (Harrison and Pio, 1983; Wall et al., 1988). Through this artefact, ammonium chloride (NH_4Cl) is released as gas while resulting in a loss of NH_4^+ and Cl^- in the respective QFF (Querol et al., 2001).

A detailed description of the chemical and mineralogical composition of the collected potential local PM sources samples (M1-M9) can be found in S.I. A.2.5 and Table A6. Some discrepancies were found between the measured values and the supposed origin from the sources samples. For example, results indicated that M4 (labelled "coal from harbour") could be other combusted matter or raw material instead of combusted coal. None of potential local PM sources have an element profile easily addressable to any of the PM samples (see section 3.5.2 for corroboration).

3.5. Source apportionment

3.5.1. According to major chemical components

The major chemical components were grouped according to Querol

et al. (2004a) in: Organic Matter (OM) + Elemental Carbon (EC), crustal (CO_3^{2-}, SiO_2, Al_2O_3, Ca, K, Mg, Fe and P_2O_5), Secondary Inorganic Aerosols (SIA) (non-marine SO_4^{2-}, NO_3^-, and NH_4^+) and Marine (Na, Cl^- and marine SO_4^{2-}). Results, shown in Fig. 4a, display a high variability in the mean contribution for each of these groups in each PM fraction.

Similar mean OM + EC levels were observed for the two campaigns for overall PM and for each PM size. Although mean and standard deviation are not adequate for describing OM + EC, since only the PM_1 dataset have a normal distribution ($p = 0.88$, Welch's *t*-test), this component represents in average about 24, 9 and 9% of each PM size by mass in cold campaign and 40, 31 and 12% in warm campaign for PM_1, $PM_{2.5}$ and PM_{10}, respectively. In order to contextualize our results, a brief comparison with previous atmospheric studies carried out at Tarragona and other cities in the world can be found in S.I. A.2.6 and S.I. A.2.7, respectively.

The crustal component represents around 30% of PM mass (Fig. 4a). Crustal ranges did not change much between campaigns, although the mean values for each PM fraction were slightly higher for the cold campaign. Crustal values for PM_1 and $PM_{2.5}$ samples do not have a normal distribution ($\alpha = 0.05$), but, if one outlier for each fraction is removed from the cold campaign dataset (ID3 for PM_1 and ID4 for $PM_{2.5}$), it is possible to confirm (by successive one way ANOVA tests) that mean crustal concentrations were $PM_{10} \geq PM_{2.5} \geq PM_1$ for both campaigns ($p < 0.05$), which points to a major geogenic origin of this component.

SIA compounds accounted for up to 11% of PM mass in the cold campaign and up to 24% in the warm campaign. SIA content showed extremely high variability (CV>50%) in each dataset (by PM size and campaign). Nevertheless, mean SIA concentrations in PM_1 were equal in both campaigns ($p = 0.91$, Welch's *t*-test), while for $PM_{2.5}$ and PM_{10} they were higher in the warm campaign ($p < 0.05$, Welch's *t*-test with $\alpha = 0.04$, once one outlier, ID6, is removed from cold PM_{10} dataset). Nitrate (80%>CV>40%) could have contributed to this high SIA variability, especially because it was detected in some PM_1 samples, in most $PM_{2.5}$ samples and in all PM_{10} samples. Mean concentration of nitrate in PM_{10} samples (1.0 μg/m^3 for campaigns, $p = 0.69$, Welch's *t*-test) is close to the annual mean value (0.9 μg/m^3) considered as characteristic of rural background locations in Spain (Querol et al., 2004a). Ammonium (75%>CV>50%) is present in some PM_{10} samples and in most $PM_{2.5}$ and PM_1 samples. In general, ammonium levels were higher or equal in warm than in cold campaign ($p < 0.05$, paired one tail Welch's *t*-test with $\alpha = 0.01$). A positive relationship between ammonium vs. sulphate + nitrate major than the hypothetical neutralization (i.e., slope = 1) of most of the acid nitrate and sulphate aerosol is observed for all PM sizes (Querol et al., 2001, S.I. Figure A12 and Pathak et al., 2009, S.I. Figure A13), although the stronger correlation ($R^2 \geq 0.8$) and closer to unity is observed for PM_1. The fact that this correlation is almost identical between ammonium and non-marine sulphate + nitrate (S.I. Figure A14) suggests a secondary formation of ammonium sulphate ($(NH_4)_2SO_4$) from primary anthropogenic gas emission sources such as road traffic or fertilizer volatilization.

Marine component (marine spray) was higher in the cold than in the warm campaign ($p < 0.05$, Welch's *t*-test). Comparing mean concentrations of marine spray in PM_{10} for both campaigns (3.9–6.0 μg/m^3), Tarragona values were higher than expected for the Mediterranean Sea (2–4 μg/m^3), closer to Atlantic Ocean Spanish locations (4–7 μg/m^3), but still lower than Canary Islands (12 μg/m^3) (Querol et al., 2004b).

The unaccounted mass of PM was estimated as the difference between de sum of previous categories (OM + EC, SIA, crustal and marine) and PM concentrations (Fig. 4a). This unaccounted mass is mainly attributed to the unaccounted water content in the structure of chemical species presents in the PM and it can be influenced by the factor used for estimating the OM + EC which varies from 1.0 to 2.5 depending on location due to specific organic compounds presence (Turpin et al., 2003; Pang et al., 2006). For our dataset, unaccounted mass represented on average 33% of PM mass, which is in accordance with previous

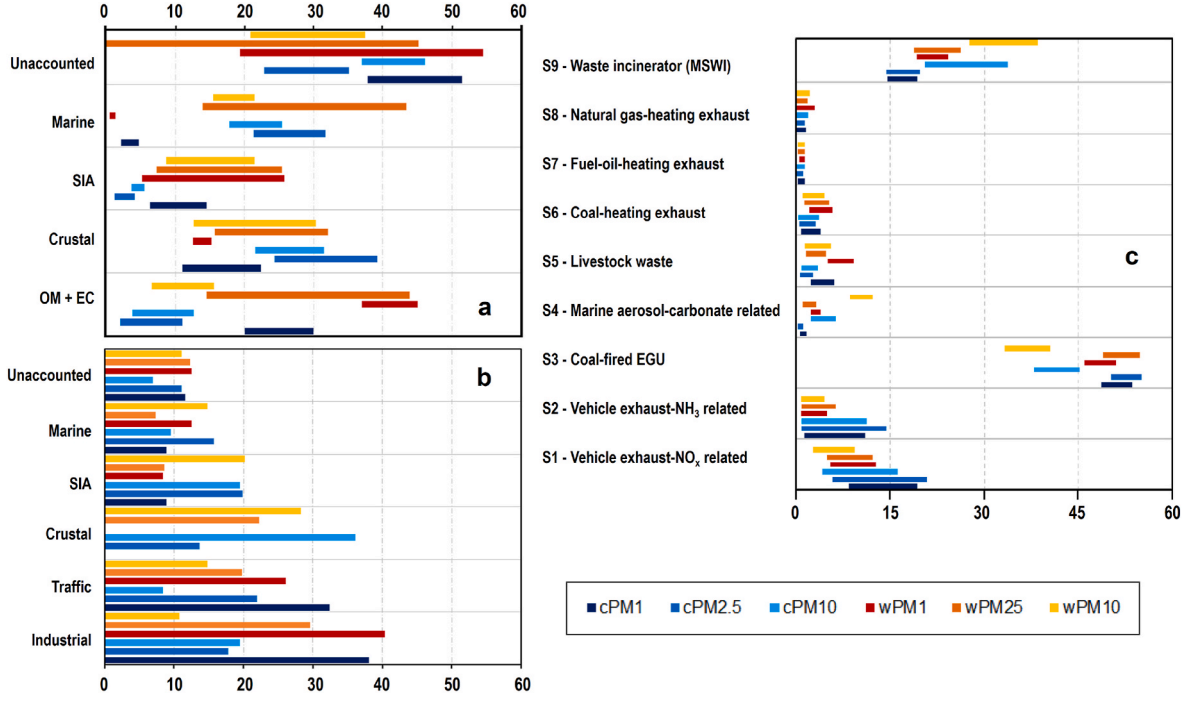

Fig. 4. Sources apportionment by: (a) Main chemical components, according to Querol et al. (2004a), contribution expressed as % in PM mass, bars represent interquartile range (b) PCA, according to the five main sources profile identified by Alastuey et al. (2007), bars represent % of variability (c) Bayesian isotope mixing model for literature sources S1–S9 (refer to Table 1 for detailed information), bars represent interquartile probability contribution (%), mean residual multiplicative error (ε) was 0.26 for $\delta^{13}C$ and 2.8 for $\delta^{15}N$, while the maximum ε values were 0.88 and 4.6, respectively. Darkest to lightest bluish and reddish bars stand for PM_1, $PM_{2.5}$ and PM_{10} in cold and warm campaigns identified by "c" and "w" prefix respectively.

studies for Catalonia (Querol et al., 2004a; Alastuey et al., 2007; Amato et al., 2016), but, it reached up to more than 60, 45 or 50% of PM mass in each PM fraction (S.I.Table A4). Nevertheless, instead of a category itself, it should be interpreted as the total uncertainty in the PM distribution according to the other four categories.

3.5.2. According to Principal Component Analysis (PCA)

PCA was applied for identifying more reliable potential sources affecting the PM composition at the studied schools. This analysis consists in performing a matrix decomposition of the PM receptors profile in two matrices: one for the sources profiles and another for the apportionments. The obtained eigenvectors correspond to the sources profiles and they should be related to some well-known pollution sources profiles by their key elements. While in most air pollution studies four to six components have been considered (Querol et al., 2001; Viana et al., 2006b; Pey, 2008; Sánchez de la Campa et al., 2010), up to seven components have been previously used for source apportionment in Tarragona's air pollution (Moreno et al., 2006; Alastuey et al., 2007). For the present dataset, an exploratory analysis of the receptor matrix indicated that only the first two components showed large eigenvalues and that up to 10 components would be required for explaining 90% of concentrations variance. The number of potential components was thus limited to four, knowing that reconstructed variance will be greater than 70%. A PCA with varimax rotation was performed to the logarithm of chemical concentrations dataset, first as a whole and then by PM size. Apportionment analysis was restricted to elements with more than 95% of confidence level in order to avoid false positive relationships (Colquhoun, 2017). Datasets with 24, 17, 16 and 14 variables (corresponding to different elements concentrations) were used in the PCA for the whole, PM_1, $PM_{2.5}$ and PM_{10} analysis, respectively. The results of KMO ($\geq$0.6) and BTS ($p < 0.001$) tests indicated a good fit for PCA (S.I. Table A9).

For all runs, PCA consistently identified four separate Principal Components (PC1 to PC4). For the whole dataset, PC1 is enriched in Pb and Zn, and PC2 in Ca, Cu, and Na. PC3 contains apportionment from Ge, Cr and Zr, while PC4 shows important contributions from Fe, Mn and Ti. Different PCA results were obtained for PM_1, $PM_{2.5}$ and PM_{10} datasets as detailed in S.I. and shown in Figure A15. The disparity of results among whole dataset, and PM_1, $PM_{2.5}$ and PM_{10} datasets could indicate that their compositions are not affected by the same set of sources or that these sources do not have the same level of relevance for each size fraction. For example, PC3 shows high C and N loadings for the three PM fractions, while the four components of the whole dataset exhibit small C loadings and N was excluded because it could not be unambiguously assigned to any component (S.I. Figure A15). A component enriched in C and N might be attributed to the presence of organic compounds such as polycyclic aromatic hydrocarbons (PAHs), polychlorinated biphenyls (PCBs), hexachlorobenzene (HCB), brominated flame retardants (BFRs), benzothiazole (BTHs), benzotriazole (BTRs) or benzenesulfonamides (BSAs). Such compounds have been previously found in $PM_{2.5}$ and PM_{10} filters in Tarragona (Mari et al., 2009; Domingo et al., 2017; Domínguez Morueco, 2018; Maceira et al., 2018), although they are likely attributed to PM_1 or smaller particles as other studies point out (e.g. Barbas et al., 2018).

Based in the PCA results and taking into account previous sources identified in Tarragona (e.g. Alastuey et al., 2007), the following five categories were built: "Industrial", which accounted for components enriched in Mn and Pb; "Crustal", for those enriched in Fe and Ti; "Marine", for those enriched in Cl and Na; "SIA", for components enriched in C; and "Traffic", for the component enriched in V for PM_1 and those enriched in Sb and Zn for $PM_{2.5}$ and PM_{10}. When one component shows significant loadings for key elements of more than one category, the component variability was equally distributed among the corresponding categories. Results are shown in Fig. 4b.

3.5.3. According to dual C and N isotope assessment

The $\delta^{13}C$ of TC in PM from the QFFs from the sampled schools ranged between −28.1‰ and −22.0‰. This range overlapped the ranges previously reported for coal mineral (−22 to −28‰, Suto and Kawashima, 2016), C3 plants (−23 to −30‰, Deines, 1980) and petroleum crude oil (−19 to −33‰, Whiticar et al., 1996) and it was similar to $\delta^{13}C$ values found in areas where fossil fuel burning occurs (−25 to −31‰, Mook et al., 1983). Significant differences ($p < 0.05$, one way ANOVA) were found between overall mean $\delta^{13}C$ values for each PM size (−26.7 ± 0.3‰, −26.7 ± 0.5‰ and −25.9 ± 1.1‰ for PM_1, $PM_{2.5}$ and PM_{10}, respectively): $\delta^{13}C$ in $PM_{10} > PM_{2.5}$ and $PM_{10} > PM_1$. For both campaigns, there were also significant differences between mean $\delta^{13}C$ values for each PM size: $\delta^{13}C$ in $PM_{10} > PM_{2.5}$ and $PM_{10} > PM_1$ ($p < 0.05$, one way ANOVA and Welch's T-test), and $PM_{2.5} \geq PM_1$ ($p = 0.18$, Welch's T-test). Thus, in general, $\delta^{13}C$ (PM_{10}) > $\delta^{13}C$ ($PM_{2.5}$) > $\delta^{13}C$ (PM_1), which points to an additional contribution in PM_{10} of coarse PM with a more enriched ^{13}C signature than PM_1 (e.g., from S4, marine carbonaceous, $\delta^{13}C \sim 0$‰). This behaviour was also observed around a cement plant (Mari et al., 2016) and is consistent with our SEM observations (i.e., presence of calcite in PM_{10} and $PM_{2.5}$, but not in PM_1).

A higher variability in $\delta^{15}N$ values was observed (+1.6 to +13.3‰), spreading more in warm than in cold campaign ($\delta^{15}N$ variation, $\Delta\delta^{15}N$ = 10.8‰ vs. 7.6‰, respectively). All this points to multiple emission sources of nitrogen or to the post-emission occurrence of secondary processes of gas to particle conversions on ambient aerosols that induce nitrogen isotope fractionation (Agnihotri et al., 2011; Sharma et al., 2015, 2022; Morera-Gómez et al., 2018). However, no significant differences ($p = 0.14$, one way ANOVA) were found between the overall mean $\delta^{15}N$ values for the three PM sizes (+9.4 ± 2‰ for PM_1, +10.3 ± 2‰ for $PM_{2.5}$ and +8.0 ± 2‰ for PM_{10}).

Comparison with previously reported isotopic data from potential emission sources was also performed in terms of $\delta^{13}C$ vs. TC and $\delta^{15}N$ vs. TN following the referential boxes of the original works (Widory et al., 2004; Widory, 2007) instead of using the values given in Table 1. Regarding the sampled potential local PM sources (M1-M8-9), only the MSWI sample (M3) fell inside the expected reference box (Fig. 5a). The disagreement between the measured and the expected isotopic composition of the potential local PM sources is probably related to the sampling approach (e.g., scratching from the tailpipe) or due to changes in the fuel composition along the time and among countries. PM_1, $PM_{2.5}$ and PM_{10} samples displayed a narrow range of $\delta^{13}C$ values, but a large variability in %TC, especially for PM_1 in warm campaign. In fact, most samples fell inside the reference box for diesel car exhaust, except three PM_{10} samples from the cold campaign (ID7, ID2 and ID5), which can be interpreted as a mixture of contributions from different sources (Fig. 5a). Attending to their $\delta^{15}N$ signature and TN content, most PM_1 samples fell within the reference area for gasoline vehicle exhaust (Fig. 5b). PM_{10} and $PM_{2.5}$ samples, in contrast, likely had also contribution from other sources, such as emissions from natural gas-heating units or diesel vehicles. Thus, this first isotopic assessment already points to a mixture of sources, probably with a remarkable contribution from vehicles exhaust.

$\delta^{15}N$ values were strong and positively correlated to TN for $PM_{2.5}$ samples in warm campaign ($r = 0.92$) and PM_{10} samples in cold campaign ($r = 0.75$), but inversely correlated to TN for $PM_{2.5}$ samples in cold campaign ($r = -0.51$). Weak correlations ($0.36 > r > 0.09$) were found for the other datasets. The correlation between $\delta^{15}N$ and ammonium content was weak ($0.33 > r > 0.11$), except for $PM_{2.5}$ samples ($r = -0.95$ for cold and 0.80 for warm campaigns). Sulphate was positive and weakly correlated with $\delta^{15}N$ for PM_1 ($0.22 > r > 0.15$), positive and moderately correlated for PM_{10} ($0.43 > r > 0.41$), inversely correlated for $PM_{2.5}$ in cold campaign ($r = -0.28$) and positive and strongly correlated for $PM_{2.5}$ in warm campaign ($r = 0.92$). All these relationships are summarised in S.I. Table A10. Strong and positive correlation between $\delta^{15}N$ and TN, ammonium or sulphate, which has been previously reported (Sharma et al., 2015, 2022; Morera-Gómez et al., 2018), suggests that secondary nitrogen is formed. The influence of secondary

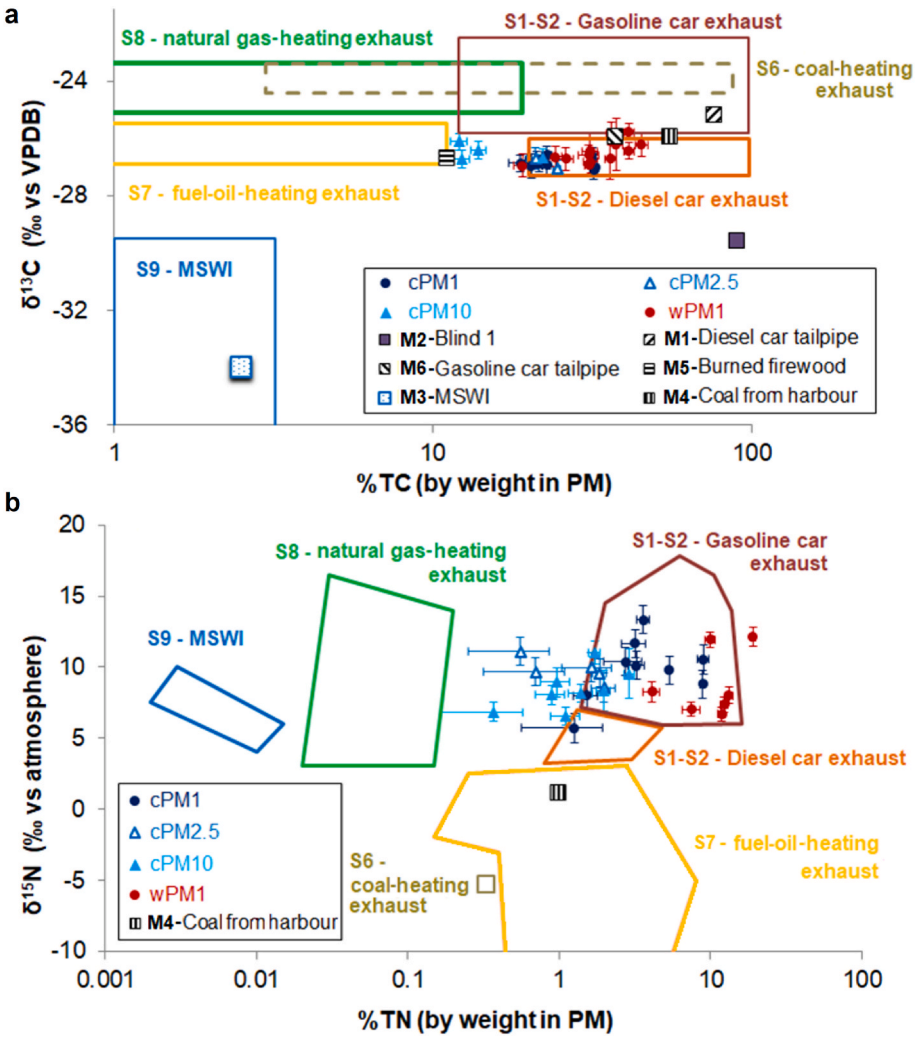

Fig. 5. Isotopic composition versus concentration of C (a) and N (b) in PM samples from Tarragona and literature reference boxes of potential pollution-source emissions according to Widory et al. (2004a) and Widory (2007), respectively.

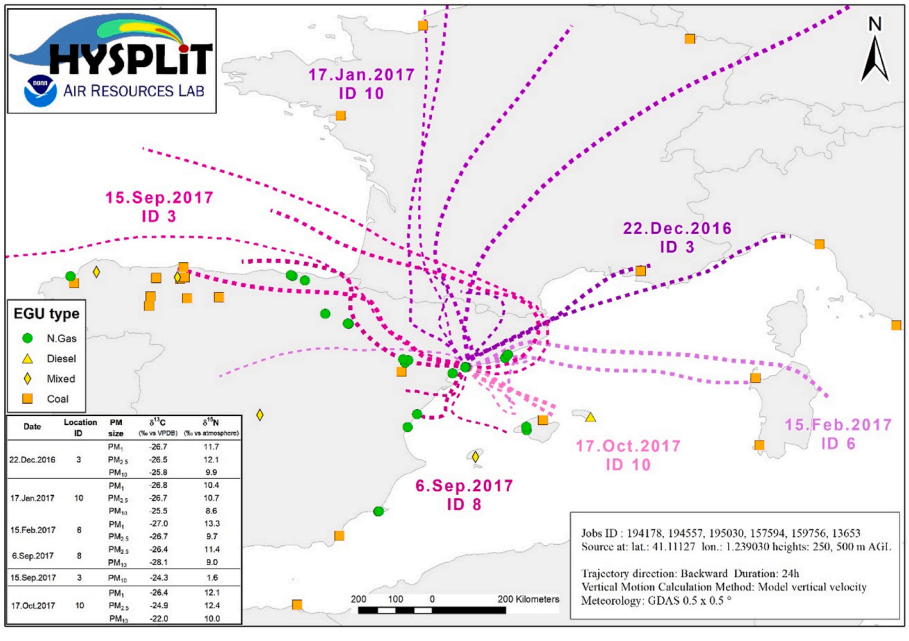

Fig. 6. Back trajectories for those sampling days with relative minimum or maximum $\delta^{15}N$ and $\delta^{13}C$ values. Location of nearest EGUs is also shown. Blue- and red-shifted purple dotted lines stand for cold and warm campaign, respectively. The increasing width of the lines correspond to 24h, 18h, 12h or 6h backward air mass trajectories. Labels stand for sampling dates and school ID. Composed from HYSPLIT Jobs ID numbers: 194178, 194557, 195030, 157594, 159756 and 13653. EGU locations taken from Global Power Plant Database (http://www.wri.org). Base map obtained from Esri, DigitalGlobe, GeoEye, and others GIS User Community in ArcGIS10.2. (For interpretation of the references to colour in this figure legend, the reader is referred to the Web version of this article.)

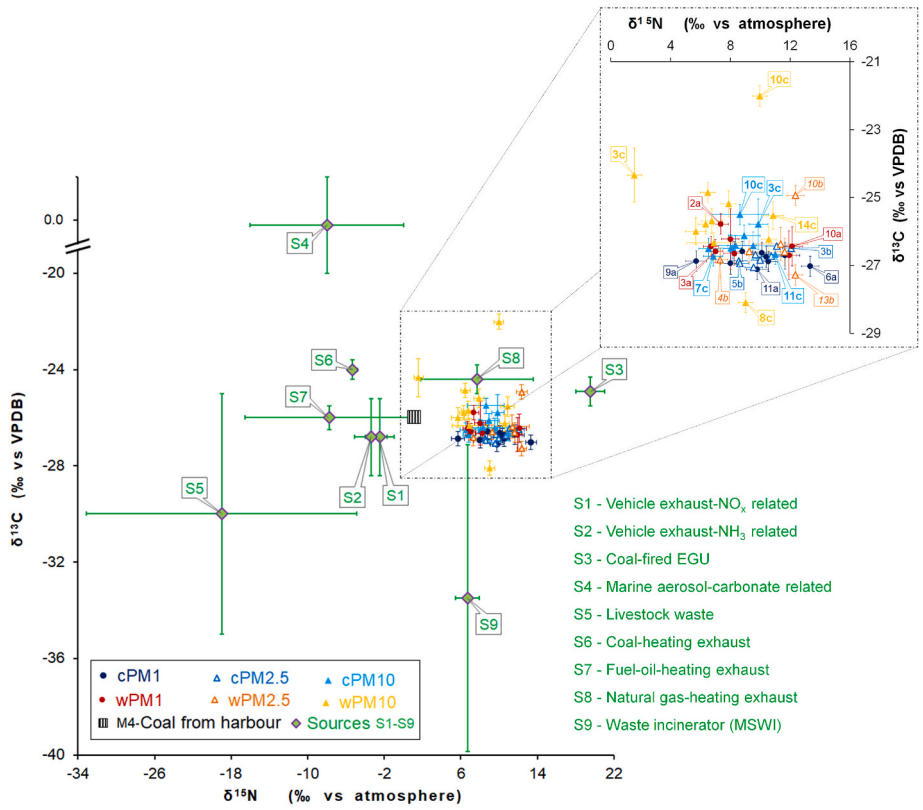

Fig. 7. Dual $\delta^{13}C$ and $\delta^{15}N$ plot for the QFFs, the sampled potential local PM sources (when possible, i.e., M4) and the reference atmospheric emission sources from literature (S1–S9, refer to Table 1 for detailed information). The close-up shows QFFs labelled according to school ID and PM size (a, b or c for PM_1, $PM_{2.5}$ or PM_{10}, respectively).

processes can also be inferred from the higher nitrogen content in PM samples than in the potential local PM sources (Fig. 3) and by the strong correlation between ammonium and sulphate content (see section 3.5.1).

If PM levels are only driven by local combustion sources or processes, PM levels should follow seasonal trends of NO_x (Querol et al., 2001). This is not the case for some locations, pointing to inputs from long-range external PM sources. For example, for ID7 (PM_{10}) and ID8 (PM_{10}) a higher PM mass in the cold campaign did not match with a change in NO_x content nor $\delta^{15}N$ value. For ID2 (PM_{10}) and ID11 (PM_{10}), a higher PM content in the cold campaign coincided with a higher $\delta^{15}N$ value and a lower NO_x content. Looking for EGUs contribution pointed by Fig. 5b, NOAA HYSPLIT back trajectories of air masses for all sampling days were thus evaluated to find potential long-range contributions to composition or PM levels. Fig. 6 shows the 24-h air mass back trajectories for those days when minimum or maximum $\delta^{15}N$ and $\delta^{13}C$ values were found. For the cold campaign, they occurred on Dec.22, Jan.17 and Feb.15 at schools ID3, ID10 and ID6, respectively, while for the warm campaign they were on Sep.6, Sep.15 and Oct.17 at schools ID8, ID3 and ID10. Two distinct groups of air mass trajectories reaching Tarragona at these dates can be observed: (1) winds originating from continental Europe (ID10 and ID3) and the Mediterranean-Sardinia (ID6) during the cold campaign, and (2) winds blowing from the Atlantic coast (ID3) and the Mediterranean-Balearic Islands (ID10) during the warm campaign. The coincidence of the observed trajectories with the location of natural gas-fired and coal-fired EGUs confirms punctual long-range contribution of EGUs to airborne PM in Tarragona.

Finally, Fig. 7 shows a dual isotope plot ($\delta^{13}C$ vs. $\delta^{15}N$) for PM samples from this study and for all potentially relevant atmospheric emission sources (Table 1), as well as the only potential local PM source sample for which both $\delta^{13}C$ and $\delta^{15}N$ could be obtained (M4). Samples clustered around −26‰ for $\delta^{13}C$ and +9‰ for $\delta^{15}N$, except three PM_{10} samples from warm campaign (Sep.05-ID8, Sep.14-ID3 and Oct.16-ID10), which showed the highest and the lowest $\delta^{13}C$ values and the lowest $\delta^{15}N$ value, respectively, commented previously with respect to 24h air masses back-trajectories. PM_1 samples from the cold campaign showed the maximum (Feb.14-ID6) and the second minimum (Jan.10-ID9) $\delta^{15}N$ values. Comparing with the isotope signature of the emission sources (S1S9), it is clear that contribution from S3 (coal-fired EGUs as those showed in Fig. 6) is needed to define a convex polygon that includes all the PM samples. Given the potential contribution from multiple atmospheric emission sources (S1–S9), their contribution must thus be addressed by a mixing model. A probabilistic mixing model such as MixSIAR seems to be more adequate than a deterministic mixing model such as EMM for evaluating as many sources as we want to contemplate here (S1–S9), because a probabilistic mixing model allows exploring source contributions iteratively.

By using the MixSIAR interface in R (Stock and Semmens, 2016; Stock et al., 2018), different mixing scenarios were evaluated to estimate the proportional contribution of the selected reference sources (S1 to S9 in Table 1) to the carbon and nitrogen isotopic signature in PM samples from the schools. The MixSIAR generated several Bayesian solutions, starting by assuming equal contribution from all sources, but then going to modify relative contributions of the sources in regular steps up to obtain an output dataset that can be statistically analysed and summarised. Through the MixSIAR interface, the Bayesian isotope mixing model was run by considering three different scenarios: (1) overall (i.e., source contributions obtained for all samples together), (2) categorised by PM size and (3) categorised first by PM size and then by campaign. The residual errors in $\delta^{13}C$ (Epsilon1, ε1) and $\delta^{15}N$ (Epsilon2, ε2) were higher for the overall scenario, while the lowest errors were obtained for the particle size nested by campaign scenario (data not shown).

The iterative Bayesian runs generate solutions for all possible situations including those which only one of the reference sources

contributes with more than 90% to the δ values for each sample, or those which all reference sources contribute less than 5% to each δ value. Thus, from all the possible Bayesian solutions (mathematical solutions), only a subgroup of solutions represents the possibility that all reference sources (S1–S9) contribute significantly to the isotopic signature of the samples. From this subgroup of solutions, in the scenario where the samples were categorised by PM size and then nested by campaign, the apportionment for the interquartile situation of the evaluated Bayesian scenarios is presented in Fig. 4c.

3.5.4. Comparison of results among methodologies

Obtained results among methodologies cannot be directly compared (please notice that bars in Fig. 4 represent different categories and they are expressed in different units in each panel).

For a better comparison to the isotopic approach, categories obtained by the main chemical components and/or the PCA were clustered. S4 in the isotopic approach, which accounts for geogenic emissions, was considered equivalent to the sum of the categories "Marine" and "EC" of the chemical approach. Their contributions (≈10%) match pretty well, except for $PM_{2.5}$ in the warm campaign, where the chemical approach estimated a contribution higher than 20%. S4 contribution is higher in PM_{10} than in $PM_{2.5}$ or PM_1, which is consistent with the results from the chemical approach, the range of trace element ratios, and what was observed by SEM. The evaluated Bayesian scenarios suggest clearly a greater marine-geogenic contribution in the warm than in the cold campaign, which could not have been distinguished as strongly by using the other approaches.

The rest of sources, other than S4, are anthropogenic and represent the main contributions for the three methodologies. S1 and S2 were considered equivalent to the "Traffic" category of the PCA. Their contributions (≈20% for PM_1 and $PM_{2.5}$, ≈15% for PM_{10}) are lower than those obtained by the PCA approach. S3, S5 and S9 can be interpreted as "Industrial" or "SIA" contribution and account for 70% of PM, in a good agreement with the results of the PCA approach. Finally, categories S6 to S8, which correspond to heating exhaust, were considered equivalent to part of the category "OM + EC" of the chemical approach. Their contribution represents at least 10% of PM.

In a more general perspective, the sources distinguished by the isotopic approach can be grouped in 2 "classical" categories: "from-combustion emission" (S1, S2, S3, S6, S7, S8 and S9, which accounted for about 70% of PM) and "from-non-combustion emission" (S4 and S5, which accounted for about 25% of PM). However, a new category combining S1, S2, S3, S5 and S9 can be built taking into account the "after-combustion" or Secondary Organic Aerosol (SOA), which plays a critical role in haze pollution in megacities (Han et al., 2015; Liu et al., 2021) and cannot be addressed by conventional source apportionment approaches (i.e., main chemical components or PCA). SOA contribution is clearly PM size-dependent and represents at least 75% of PM_1 and 60% of PM_{10}. Particles generated from waste incinerator (MSWI) and coal-fired EGU emissions explain up to 50% of the PM mass for each PM size (≈50% for PM_1 and $PM_{2.5}$, ≈40% PM_{10}). This means that secondary particles (SIA and SOA) are the most significant component in such complex emission environments.

Furthermore, the dual isotope mixing model (Fig. 4c) allows reducing the uncertainty in PM source apportionment, resulting in a small residual error (5%) compared to the high "unaccounted" PM obtained by the other two methods: about 45% by the main chemical components (Figs. 4a) and 10% by the PCA (Fig. 4b). For example, in the case of PM_1, where more than 40% of the mass is unaccounted by using the main chemical components, and although PCA shows more information because a similar amount (almost 40% of PM_1 variability) can be attributed to industrial sources, only with the isotopic approach is revealed that more than 60% of PM_1 probably comes from a blend of coal-fired EGU and waste incinerator.

4. Conclusions

In this study, different approaches were applied and compared for source apportionment of three PM fractions (PM_1, $PM_{2.5}$ and PM_{10}) in a complex urban and industrial site. For the first time, a dual isotope approach combined with a Bayesian isotope mixing model and considering air masses back trajectories for possible long-distance contributions were used to interpret and quantify the different seasonal source apportionment of the three PM fractions.

Methodologically, the dual-isotope mixing model allowed us differentiating geogenic from anthropogenic sources and contributions, which could not have been possible using conventional approaches such as chemical components or PCA without the help of other techniques. Secondly, it has significantly reduced the "unaccounted" contribution in major PM components by accounting oxygenated (secondary) compounds, which could not be considered using the conventional chemical approaches. Third, the remarkable seasonal differences in isotopic signatures permitted to distinguish a higher contribution from waste incinerator (PM_1 and $PM_{2.5}$) and marine aerosol (PM_1, $PM_{2.5}$ and PM_{10}) in the warm campaign. All in all, the advantages of this approach are accomplished with less resources both for pre- and post-analysis than other methodologies.

From a practical point of view, this comprehensive study integrating elemental, isotopic, and mathematical source apportionment solutions has been validated in a complex urban and industrial city allowing apportioning the contribution of the main PM sources. Results indicated that two kinds of sources mainly contributed to PM samples in Tarragona city: local and direct sources (e.g., road traffic and industrial sources) and external or indirect (e.g., long-range, SOA and SIA) sources. Emissions from coal-fired EGUs (up to 50%) and road traffic (15–20%) were found to be the major source contributions, followed by waste incinerator (20–30%) and livestock emissions (5–10%). Most of the road traffic emission is composed by gasoline and diesel combustion, while in cold campaign also contribution from vehicular natural gas combustion could be addressed. Coal-fired EGU emissions and road traffic mainly contributed to PM_1, whereas $PM_{2.5}$ and PM_{10} are also related to waste incinerator, livestock waste and marine aerosol. The contribution of coal-fired EGU emissions was inferred from trace element ratios, isotopic composition and air masses back trajectories. In future works, it could be addressed to what extent coal combustion contribution is also due to local burning of wood or stubble (from heating, forestry or agriculture practices) by analysing for example the PAHs content.

CRediT authorship contribution statement

Edson Plasencia Sánchez: Investigation, Conceptualization, Methodology, Formal analysis, Writing – original draft, Visualization. **Francisco Sánchez-Soberón:** Investigation, Data curation, Writing – review & editing. **Joaquim Rovira:** Investigation, Methodology, Data curation, Writing – review & editing. **Jordi Sierra:** Investigation, Data curation, Writing – review & editing. **Marta Schuhmacher:** Conceptualization, Funding acquisition, Writing – review & editing. **Albert Soler:** Conceptualization, Funding acquisition, Project administration. **Clara Torrentó:** Conceptualization, Methodology, Supervision, Writing – review & editing. **Mònica Rosell:** Conceptualization, Methodology, Supervision, Writing – review & editing.

Declaration of competing interest

The authors declare that they have no known competing financial interests or personal relationships that could have appeared to influence the work reported in this paper.

Data availability

Data will be made available on request.

Acknowledgements

The present research work was funded by UltraPAR [CTM 2015-65303-P], REMEDIATION [CGL 2014-57215-C4-1-R] and PACE [CGL 2017-87216-C4-1-R] projects from Spanish Ministry of Economy and Competitiveness (MINECO), co-financed by the European Union through the European Regional Development Fund (AEI/FEDER, UE). This work was also partly supported by the *Generalitat de Catalunya* through the Consolidate Research Group [2017-SGR-1733] and current E. Plasencia Sánchez PhD grant [2020 FISDU 00567]. He was earlier supported by the Peruvian Government credit-fellowship "Reto Excelencia" [036–2015]. J. Rovira received a postdoctoral fellowship from "Juan de la Cierva-incorporación" program of the Spanish Ministry of Science, Innovation and Universities (MCIU) [IJC 2018-035126-I]. We also thank the technical support from CCiT-UB and the undergraduated student Manel Sánchez Guijarro for his help in the mineralogical characterisation part of his bachelor's degree final project.

Appendix A. Supplementary data

Supplementary data to this article can be found online at https://doi.org/10.1016/j.atmosenv.2022.119449.

References

AEQT. Associació empresarial Química de Tarragona. HomePage. Avalable from. http://www.aeqtonline.com. (Accessed 10 June 2019).

Agnihotri, R., Mandal, T.K., Karapurkar, S.G., Naja, M., Gadi, R., Ahammmed, Y.N., Kumar, A., Saud, T., Saxena, M., 2011. Stable carbon and nitrogen isotopic composition of bulk aerosols over India and northern Indian Ocean. Atmos. Environ. 45, 2828–2835.

Aguilera, J., Whigham, L., 2018. Using the 13C/12C carbon isotope ratio to characterise the emission sources of airborne particulate matter: a review of literature. Isot. Environ. Health Stud. 54, 1–15.

Ahn, J.E., Karlsson, M.O., Dunne, A., Ludden, T.M., 2008. Likelihood based approaches to handling data below the quantification limit using NONMEM VI. J. Pharmacokinet. Pharmacodyn. 35, 401–421.

Alastuey, A., Moreno, N., Querol, X., Viana, M., Artiñano, B., Luaces, J.A., Basora, J., Guerra, A., 2007. Contribution of harbour activities to levels of particulate matter in a harbour area: hada Project-Tarragona Spain. Atmos. Environ. 41, 6366–6378.

Altieri, K.E., Hastings, M.G., Gobel, A.R., Peters, A.J., Sigman, D.M., 2013. Isotopic composition of rainwater nitrate at Bermuda: the influence of air mass source and chemistry in the marine boundary layer. J. Geophys. Res. Atmos. 118, 19 11–304.

Alves, C.A., Evtyugina, M., Vicente, A.M.P., Vicente, E.D., Nunes, T.V., Silva, P.M.A., Duarte, M.A.C., Pio, C.A., Amato, F., Querol, X., 2018. Chemical profiling of PM10 from urban road dust. Sci. Total Environ. 634, 41–51.

Amato, F., Alastuey, A., Karanasiou, A., Lucarelli, F., Nava, S., Calzolai, G., Severi, M., Becagli, S., Gianelle, V.L., Colombi, C., Alves, C., Custodio, D., Nunes, T., Cerqueira, M., Pio, C., Eleftheriadis, K., Diapouli, E., Reche, C., Minguillón, M.C., Manousakas, M.-I., Maggos, T., Vratolis, S., Harrison, R.M., Querol, X., 2016. AIRUSE-LIFE+: a harmonized PM speciation and source apportionment in five southern European cities. Atmos. Chem. Phys. 16, 3289–3309.

Barbas, B., De la Torre, A., Sanz, P., Navarro, I., Artíñano, B., Martínez, M.A., 2018. Gas/particle partitioning and particle size distribution of PCDD/Fs and PCBs in urban ambient air. Sci. Total Environ. 624, 170–179.

Bornemann, A., Pirkenseer, C.M., De Deckker, P., Speijer, R.P., 2012. Oxygen and carbon isotope fractionation of marine ostracod calcite from the eastern Mediterranean Sea. Chem. Geol. 310–311, 114–125.

Calvello, M., Caggiano, R., Esposito, F., Lettino, A., Sabia, S., Summa, V., Pavese, G., 2017. IMAA (Integrated Measurements of Aerosol in Agri valley) campaign: multi-instrumental observations at the largest European oil/gas pre-treatment plant area. Atmos. Environ. 169, 297–306.

Colquhoun, D., 2017. The reproducibility of research and the misinterpretation of *p*-values. R. Soc. Open Sci. 4, 171085.

Coplen, T.B., Brand, W.A., Ghere, M., Gröning, M., Meijer, H.A.J., Toman, B., Verkouteren, R.M., 2006. New guidelines for δ13C measurements. Anal. Chem. 78, 2439–2441.

Davidson, C.I., Phalen, R.F., Solomon, P.A., 2005. Airborne particulate matter and human health: a review. Aerosol. Sci. Technol. 39 (8), 737–749.

Deines, P., 1980. The isotopic composition of reduced organic carbon. In: Fritz, P., Fontes, J.Ch (Eds.), Handbook of Environmental Isotope Geochemistry, vol. 1. Elsevier, New York, pp. 329–406.

DGT, 2020. Dirección General de Tráfico - Ministerio del Interior, Anuario Estadístico General 2020. Available from: http://www.dgt.es/es. (Accessed 3 May 2022).

Di Palma, A., Capozzi, F., Agrelli, D., Amalfitano, C., Giordano, S., Spagnuolo, V., Adamo, P., 2018. Geochemistry and carbon isotopic ratio for assessment of PM10 composition, source and seasonal trends in urban environment. Environ. Pollut. 239, 590–598.

Domingo, J.L., García, F., Nadal, M., Schuhmacher, M., 2017. Autopsy tissues as biological monitors of human exposure to environmental pollutants. A case study: concentrations of metals and PCDD/Fs in subjects living near a hazardous waste incinerator. Environ. Res. 154, 269–274.

Domínguez Morueco, N., 2018. Environmental Levels of PAHs and Other SVOCs in a Petrochemical Area. *Combining Monitoring and Modelling Tools* (Doctoral Thesis Dissertation). Universitat Rovira i Virgili, Tarragona, Catalonia, Spain.

Domínguez-Morueco, N., Augusto, S., Trabalón, L., Pocurull, E., Borrull, F., Schuhmacher, M., Domingo, J.L., Nadal, M., 2017. Monitoring PAHs in the petrochemical area of Tarragona County, Spain: comparing passive air samplers with lichen transplants. Environ. Sci. Pollut. Res. 24, 11890–11900.

Draxler, R.R., Rolph, G.D., 2003. HYSPLIT (HYbrid Single-Particle Lagrangian Integrated Trajectory) Model Access via NOAA ARL READY. Website. http://www.arl.noaa.gov/ready/hysplit4.html.

Drever, J.J., 1982. The Geochemistry of Natural Waters. Prentice-Hall Inc., Englewood Cliffs, NJ.

Ec – European Council, 2008. Directive 2008/50/EC of the European Parliament and of the Council of 21 May 2008 on Ambient Air Quality and Cleaner Air for Europe. Official Journal of the European Union.

Ertel, J.R., Hedges, J.I., 1985. Sources of sedimentary humic substances: vascular plant debris. Geochem. Cosmochim. Acta 49, 2097–2107.

Fan, Z., Lin, L., 2011. Exposure science: contaminant mixtures. In: Nriagu, J.O. (Ed.), Encyclopedia of Environmental Health. Elsevier, pp. 645–656.

Felix, J.D., Elliott, E.M., 2014. Isotopic composition of passively collected nitrogen dioxide emissions: vehicle, soil and livestock source signatures. Atmos. Environ. 92, 359–366.

Felix, J.D., Elliott, E.M., Shaw, S.L., 2012. Nitrogen isotopic composition of coal-fired power plant NO_x: influence of emission controls and implications for global emission inventories. Environ. Sci. Technol. 46, 3528–3535.

Felix, J.D., Elliott, E.M., Gish, T., McConnell, L., Shaw, S., 2013. Characterizing the isotopic composition of atmospheric ammonia emission sources using passive samplers and a combined oxidation bacterial denitrifier isotope ratio mass spectrometer method. Rapid Commun. Mass Spectrom. 27, 2239–2246.

Ferin, J., Oberdorster, G., Penney, D.P., 1992. Pulmonary retention of ultrafine and fine particles in rats. Am. J. Respir. Cell Mol. Biol. 6, 535–42.

Font, A., Hoogh, K., Leal-Sanchez, M., Ashworth, D.C., Brown, R.J.C., Hansell, A.L., Fuller, G.W., 2015. Using metal ratios to detect emissions from municipal waste incinerators in ambient air pollution data. Atmos. Environ. 113, 177–186.

Freyer, H.D., 1978. Preliminary 15N studies on atmospheric nitrogenous trace gases. Pure Appl. Geophys. 116, 393–404.

Friedlander, S.K., 1973. Chemical element balances and identification of air pollution sources. Environ. Sci. Technol. 7 (3), 235–240.

GENCAT, 2018. Generalitat de Catalunya - Institut d'Estadística de Catalunya, Servei Meteorològic de Catalunya, Temperaturas Mínimas. Available from: https://www.idescat.cat. (Accessed 14 June 2020), 2020.

GENCAT, 2022. Generalitat de Catalunya - Institut d'Estadística de Catalunya, Travellers, overnight stays and occupancy rate - 2018. Available from. https://www.idescat.cat. (Accessed 18 January 2022).

GENCAT – Generalitat de Catalunya, 2019a. Dades obertes - Xarxa de Vigilància i Previsió de la Contaminació Atmosfèrica. Available from: https://analisi.transparenciacatalunya.cat. (Accessed 10 June 2019).

GENCAT – Generalitat de Catalunya, 2019b. Institut Catalá de Energía, Noticia del 23/07/2018. Available from: http://icaen.gencat.cat/es/detalls/noticies/20190723_noti_biomassa_creix. (Accessed 27 October 2019).

GGICAS - Institute of Geology and Geophysics, Chinese Academy of Sciences, 1981. Concise Handbook of Geochemistry. Scientific Press, Beijing.

Han, T., Liu, X., Zhang, Y., Qu, Y., Zeng, L., Hu, M., Zhu, T., 2015. Role of secondary aerosols in haze formation in summer in the Megacity Beijing. J. Environ. Sci. 31, 51–60.

Harrison, R.M., Pio, C., 1983. Size differentiated composition of inorganic aerosol of both marine and polluted continental origin. Atmos. Environ. 17, 1733–1738.

Heaton, T.H.E., 1987. 15N/14N ratio of nitrate and ammonium in rain of Pretoria, South Africa. Atmos. Environ. 21, 843–852.

Hulskotte, J.H.J., Roskam, G.D., Denier van der Gon, H.A.C., 2014. Elemental composition of current automotive braking materials and derived air emission factors. Atmos. Environ. 99, 436–445.

Iijima, A., Sato, K., Yano, K., Tago, H., Kato, M., Kimura, H., Furuta, N., 2007. Particle size and composition distribution analysis of automotive brake abrasion dusts for the evaluation of antimony sources of airborne particulate matter. Atmos. Environ. 41, 4908–4919.

INE – Instituto Nacional de Estadística, 2018. Población por provincia. Available from: http://www.ine.es. (Accessed 10 June 2019), 2019.

Jakeman, A.J., Voinov, A.A., Rizzoli, A.E., Chen, S.H., 2008. Environmental Modelling, Software and Decision Support: State of the Art and New Perspective. Elsevier Science, ISBN 0080915302.

Kabala, C., Singh, B.R., 2001. Fractionation and mobility of copper, P, and zinc in soil profiles in the vicinity of a copper smelter. J. Environ. Qual. 30, 485–492.

Kunwar, B., Kawamura, K., Zhu, Ch, 2016. Stable carbon and nitrogen isotopic compositions of ambient aerosols collected from Okinawa Island in the western North Pacific Rim, an outflow region of Asian dusts and pollutants. Atmos. Environ. 131, 243–253.

Leng, X., Qian, X., Yang, M., Wang, Ch, Li, H., Wang, J., 2018. Leaf magnetic properties as a method for predicting heavy metal concentrations in PM2.5 using support vector machine: a case study in Nanjing, China. Environ. Pollut. 242, 922–930.

Li, T., Li, J., Jiang, H., Chen, D., Zong, Z., Tian, C., Zhang, G., 2020. Source apportionment of PM2.5 in guangzhou based on an approach of combining positive

matrix factorization with the bayesian mixing model and radiocarbon. Atmosphere 11 512.
Lim, S., Lee, M., Czimczik, C.I., Joo, T., Holden, S., Mouteva, G., Santos, G.M., Xu, X., Walker, J., Kim, S., Kim, H.S., Lee, S., 2019. Source signatures from combined isotopic analyses of $PM_{2.5}$ carbonaceous and nitrogen aerosols at the peri-urban Taehwa Research Forest, South Korea in summer and fall. Sci. Total Environ. 655, 1505–1514.
Lin, C.C., Chen, S.J., Huang, K.L., Hwang, W.I., Chang-Chien, G.P., Lin, W.Y., 2005. Characteristics of metals in nano/ultrafine/fine/coarse particles collected beside a heavily trafficked road. Environ. Sci. Technol. 39, 8113–8122.
Liu, H.Y., Dunea, D., Iordache, S., Pohoata, A., 2018. A review of airborne particulate matter effects on young children's respiratory symptoms and diseases. Atmosphere, 9 4 150.
Liu, J., Chu, B., Chen, T., Zhong, C., Liu, C., Ma, Q., Ma, J., Zhang, P., He, H., 2021. Secondary organic aerosol formation potential from ambient air in beijing: effects of atmospheric oxidation capacity at different pollution levels. Environ. Sci. Technol. 55, 4565–4572.
López-Veneroni, D., 2009. The stable carbon isotope composition of $PM_{2.5}$ and PM_{10} in Mexico City Metropolitan Area air. Atmos. Environ. 43, 4491–4502.
Maceira, A., Marce, R.M., Borrull, F., 2018. Occurrence of benzothiazole, benzotriazole and benzenesulfonamide derivates in outdoor air particulate matter samples and human exposure assessment. Chemosphere 193, 557–566.
Macharia, A.N., Uno, K.T., Cerling, T.E., Brown, F.H., 2012. Isotopically distinct modern carbonates in abandoned livestock corrals in northern Kenya. J. Archaeol. Sci. 39, 2198–2205.
MAPA – Ministerio de Agricultura, 2020. Pesca y Alimentación, Boletín Mensual de Estadísticas – Mayo 2020. Available from: http://mapa.gob.es. (Accessed 13 June 2020), 2020.
Mari, M., Nadal, M., Schuhmacher, M., Domingo, J.L., 2009. Exposure to heavy metals and PCDD/Fs by the population living in the vicinity of a hazardous waste landfill in Catalonia, Spain: health risk assessment. Environ. Int. 35 (7), 1034–1039.
Mari, M., Sánchez-Soberón, F., Audí-Miró, C., Van Drooge, B.L., Soler, A., Grimalt, J.O., Schuhmacher, M., 2016. Source apportionment of inorganic and organic PM in the ambient air around a cement plant: assessment of complementary tools. Aerosol Air Qual. Res. 16, 3230–3242.
Mbengue, S., Alleman, L.Y., Flament, P., 2014. Size-distributed metallic elements in submicronic and ultrafine atmospheric particles from urban and industrial areas in northern France. Atmos. Res. 135, 35–47.
Mbengue, S., Alleman, L.Y., Flament, P., 2017. Metal-bearing fine particle sources in a coastal industrialized environment. Atmos. Res. 183, 202–211.
Meyers, P.A., 1994. Preservation of elemental and isotopic source identification of sedimentary organic matter. Chem. Geol. 144, 289–302.
Millán-Martínez, M., Sánchez-Rodas, D., de la Campa, A.S., Alastuey, A., Querol, X., De la Rosa, J.D., 2021. Source contribution and origin of PM10 and arsenic in a complex industrial region (Huelva, SW Spain). Environ. Pollut. 274, 116268.
Miyazaki, Y., Kawamura, K., Sawano, M., 2010. Size distributions of organic nitrogen and carbon in remote marine aerosols: evidence of marine biological origin based on their isotopic ratios. Geophys. Res. Lett. 37, L06803.
Mocak, J., Bond, A.M., Mitchell, S., Scollary, G., 1997. A statistical overview of standard (IUPAC and ACS) and new procedures for determining the limits of detection and quantification: application to voltammetric and stripping techniques. Pure Appl. Chem. 69 (2), 297–328.
Mook, W.G., Koopmans, M., Carter, A.F., Keeling, C.D., 1983. Seasonal, latitudinal, and secular variations in the abundance and isotopic ratios of atmospheric carbon dioxide: 1. Results from land stations. J. Geophys. Res. Oceans 88, 10915–10933.
Morawska, L., Zhang, J., 2002. Combustion sources of particles. 1. Health relevance and source signatures. Chemosphere 49, 1045–1058.
Moreno, T., Querol, X., Alastuey, A., Viana, M., Salvador, P., Sanchez de la Campa, A., Artiñano, B., de la Rosa, J., Gibbons, W., 2006. Variations in atmospheric PM trace metal content in Spanish towns: illustrating the chemical complexity of the inorganic urban aerosol cocktail. Atmos. Environ. 40, 6791–6803.
Moreno, T., Karanasiou, A., Amato, F., Lucarelli, F., Nava, S., Calzolai, G., Chiari, M., Coz, E., Artíñano, B., Lumbreras, J., Borge, R., Boldo, E., Linares, C., Alastuey, A., Querol, X., Gibbons, W., 2013. Daily and hourly sourcing of metallic and mineral dust in urban air contaminated by traffic and coal-burning emissions. Atmos. Environ. 68, 33–44.
Morera-Gómez, Y., Santamaría, J.M., Elustondo, D., Alonso-Hernández, C.M., Widory, D., 2018. Carbon and nitrogen isotopes unravels sources of aerosol contamination at Caribbean rural and urban coastal sites. Sci. Total Environ. 642, 723–732.
Muránszky, G., Óvári, M., Virág, I., Csiba, P., Dobai, R., Záray, G., 2011. Chemical characterization of PM10 fractions of urban aerosol. Microchem. J. 98, 1–10.
Olmo, N.R.S., do Nascimento Saldiva, P.H., Braga, A.L.F., Lin, C.A., de Paula Santos, U., Pereira, L.A.A., 2011. A review of low-level air pollution and adverse effects on human health: implications for epidemiological studies and public policy. Clinics 66, 4 681–690.
Pang, Y., Turpin, B.J., Gundel, L.A., 2006. On the importance of organic oxygen for understanding organic aerosol particles. Aerosol Sci. Technol. 40, 2 128–133.
Parnell, C.A., Phillips, L.D., Bearhop, S., Semmens, X.B., Ward, J.E., Moore, W.J., Jackson, L.A., Grey, J., Kelly, J.D., Inger, R., 2013. Bayesian stable isotope mixing models. Environmetrics 24, 387–399.
Pathak, R.K., Wu, W.S., Wang, T., 2009. Summertime $PM_{2.5}$ ionic species in four major cities of China: nitrate formation in an ammonia-deficient atmosphere. Atmos. Chem. Phys. 9 (5), 1711–1722.
Pey, J., 2008. Caracterización fisico-química de los aerosoles atmosféricos en el Mediterráneo Occidental (Doctoral dissertation in Spanish). Universitat Politècnica de Catalunya, Barcelona, Catalonia, Spain.
Phillips, L.D., Gregg, W.J., 2003. Source partitioning using stable isotopes: coping with too many sources. Oecologia 136, 261–269.
Puertos del Estado, 2021. SIMAR Data Base. Available from: https://www.puertos.es. (Accessed 23 July 2021).
Puig, R., Folch, A., Menció, A., Soler, A., Mas-Pla, J., 2013. Multi-isotopic study (^{15}N, ^{34}S, ^{18}O, ^{13}C) to identify processes affecting nitrate and sulphate in response to local and regional groundwater mixing in a large-scale flow system. Appl. Geochem. 32, 129–141.
Querol, X., Amato, F. (Eds.), 2017. Guide Book: Measures to Improve Urban Air Quality. AIRUSE LIFE Project, p. 175.
Querol, X., Alastuey, A., Rodriguez, S., Plana, F., Ruiz, C.R., Cots, N., Massague, G., Puig, O., 2001. PM10 and PM2.5 source apportionment in the Barcelona Metropolitan area, Catalonia, Spain. Atmos. Environ. 35, 6407–6419.
Querol, X., Alastuey, A., Viana, M., Rodriguez, S., Artiñano, B., Salvador, P., Garcia do Santos, S., Fernandez Patier, R., Ruiz, C.R., de la Rosa, J., Sanchez de la Campa, A., Menendez, M., Gil, J.I., 2004a. Speciation and origin of PM10 and PM2.5 in Spain. Aerosol Science 35, 1151–1172.
Querol, X., Alastuey, A., Ruiz, C.R., Artiñano, B., Hansson, H.C., Harrison, R.M., Buringh, E., Ten Brink, H.M., Lutz, M., Bruckmann, P., Straehl, P., Schneider, J., 2004b. Speciation and origin of PM10 and PM2.5 in selected European cities. Atmos. Environ. 38, 6547–6555.
Querol, X., Harrison, R.M., Hester, R.E. (Eds.), 2016. Airborne Particulate Matter: Sources, Atmospheric Processes and Health. Royal Society of Chemistry, p. 387.
Redfield, A.C., 1958. The biological control of chemical factors in the environment. Am. Sci. 46, 205–222.
Rovira, J., Sierra, J., Nadal, M., Schuhmacher, M., Domingo, J.L., 2018. Main components of PM10 in an area influenced by a cement plant in Catalonia, Spain: seasonal and daily variations. Environ. Res. 165, 201–209.
Salvi, S., 2007. Health effects of ambient air pollution in children. Paediatr. Respir. Rev. 8, 4 275–280.
Sánchez de la Campa, A., De la Rosa, J., González-Castanedo, Y., Fernández-Camacho, R., Alastuey, A., Querol, X., Pio, C., 2010. High concentrations of heavy metals in PM from ceramic factories of Southern Spain. Atmos. Res. 96, 633–644.
Sánchez-Soberón, F., Rovira, J., Mari, M., Sierra, J., Nadal, M., Domingo, J.L., Schuhmacher, M., 2015. Main components and human health risks assessment of PM_{10}, $PM_{2.5}$, and PM_1 in two areas influenced by cement plants. Atmos. Environ. 120, 109–116.
Sánchez-Soberón, F., Cuykx, M., Serra, N., Linares, V., Bellés, M., Covaci, A., Schuhmacher, M., 2018. In-vitro metabolomics to evaluate toxicity of particulate matter under environmentally realistic conditions. Chemosphere 209, 137–146.
Sánchez-Soberón, F., Rovira, J., Sierra, J., Mari, M., Domingo, J.D., Schuhmacher, M., 2019. Seasonal characterization and dosimetry-assisted risk assessment of indoor particulate matter ($PM_{10\text{-}2.5}$, $PM_{2.5\text{-}0.25}$, and $PM_{0.25}$) collected in different schools. Environ. Res. 175, 287–296.
Sen, I.S., Bizimis, M., Tripathi, S.N., Paul, D., 2016. Lead isotopic fingerprinting of aerosols to characterize the sources of atmospheric lead in an industrial city of India. Atmos. Environ. 129, 27–33.
Sharma, S.K., Karapurkar, S.G., Shenoy, D.M., Mandal, T.K., 2022. Stable carbon and nitrogen isotopic characteristics of $PM_{2.5}$ and PM_{10} in Delhi, India. J. Atmos. Chem. 79, 67–79.
Sharma, S.K., Mandal, T.K., Shenoy, D.M., Bardhan, P., Srivastava, M.K., Chatterjee, A., Saxena, M., Saraswati Singh, B.P., Ghosh, S.K., 2015. Variation of stable carbon and nitrogen isotopic composition of PM10 at urban sites of indo gangetic plain (IGP) of India. Bull. Environ. Contam. Toxicol. 95, 661–669.
Shepard, D., 1968. A two-dimensional interpolation function for irregularly-spaced data. In: Proceedings of the 1968 23rd ACM National Conference. Association for Computing Machinery, pp. 517–524.
Souto-Oliveira, C.E., Babinski, M., Araújo, D.F., Andrade, M.F., 2018. Multi-isotopic fingerprints (Pb, Zn, Cu) applied for urban aerosol source apportionment and discrimination. Sci. Total Environ. 626, 1350–1366.
Stock, B.C., Semmens, B.X., 2016. MixSIAR GUI User Manual - Version 3.1. Available from: http://github.com. (Accessed 10 June 2019).
Stock, B.C., Jackson, A.L., Ward, E.J., Parnell, A.C., Phillips, D.L., Semmens, B.X., 2018. Analyzing mixing systems using a new generation of Bayesian tracer mixing models. PeerJ 6, e5096.
Suto, N., Kawashima, H., 2016. Global mapping of carbon isotope ratios in coal. J. Geochem. Explor. 167, 12–19.
Tauler, R., Viana, M., Querol, X., Alastuey, A., Flight, R.M., Wentzell, P.D., Hopke, P.K., 2009. Comparison of the results obtained by four receptor modelling methods in aerosol source apportionment studies. Atmos. Environ. 43, 3989–3997.
Taylor, S.R., McLennan, S.M., 1985. The Continental Crust: its Composition and Evolution. Blackwell Scientific Publications, Oxford, Boston, Palo Alto, Victoria.
Thurston, G.D., 2000. Particulate Matter and Sulfate: Evaluation of Current California Air Quality Standards with Respect to Protection of Children. California Air Resources Board, California Office of Environmental Health Hazard Assessment.
Turpin, B.J., Saxena, P., Andrews, E., 2003. Measuring and simulating particulate organics in the atmosphere: problems and prospects. Atmos. Environ. 34, 2983–3013.
US-EPA – United States Environmental Protection Agency, 1996. Air Quality Criteria for Particulate Matter. EPA/600/P-95/001aF.
Viana, M., 2003. Niveles, composición y origen del material particulado atmosférico en los sectores norte y este de la península ibérica y canarias (Doctoral dissertation in Spanish). Universidad de Barcelona, Barcelona, Catalonia, Spain.

Viana, M., Querol, X., Alastuey, A., 2006a. Chemical characterisation of PM episodes in NE Spain. Chemosphere 62, 947–956.
Viana, M., Querol, X., Alastuey, A., Gil, J.I., Menéndez, M., 2006b. Identification of PM sources by principal component analysis (PCA) coupled with wind direction data. Chemosphere 65, 2411–2418.
Viana, M., Kuhlbusch, T.A.J., Querol, X., Alastuey, A., Harrison, R.M., Hopke, P.K., Winiwarter, W., Vallius, M., Szidat, S., Prévôt, A.S.H., Hueglin, C., Bloemen, H., Wåhlin, P., Vecchi, R., Miranda, A.I., Kasper-Giebl, A., Maenhaut, W., Hitzenberger, R., 2008. Source apportionment of particulate matter in Europe: a review of methods and results. Aerosol Science 39, 827–849.
Volkov, A., Serafimovski, T., Galymov, A., Leksin, A., 2017. Prospects of discovery of new deposits of lead and zinc in the republic of Macedonia. Geol. Maced. 31 1 41–48.
Wakamatsu, S., Utsunomiya, A., Suk Han, J., Mori, A., Uno, I., Uehara, K., 1996. Seasonal variation in atmospheric aerosols concentration covering Northern Kyushu, Japan and Seoul, Korea. Atmos. Environ. 30 13, 2343–2354.
Wall, S.M., John, W., Ondo, J.L., 1988. Measurement of aerosol size distribution for nitrate and major ionic species. Atmos. Environ. 22, 1649–1656.
Walters, W.W., Goodwin, S.R., Michalski, G., 2015. Nitrogen stable isotope composition ($\delta^{15}N$) of vehicle emitted NOx. Environ. Sci. Technol. 49, 2278–2285.
Wang, Y., Liu, X., Song, W., Yang, W., Han, B., Dou, X., Zhao, X., Song, Z., Liu, C., Bai, Z., 2017. Source appointment of nitrogen in PM2.5 based on bulk δ15N signatures and a Bayesian isotope mixing model. Tellus Ser. B, 69 1299672.
Watson, G.J., Zhu, T., Chow, C.J., Engelbrecht, J., Fujita, M.E., Wilson, E.W., 2002. Receptor modeling application framework for particle source apportionment. Chemosphere 49, 1093–1136.
Weng, H., Zhang, H., Chen, X., Wu, N., 2003. The stability of the relative content ratios of Cu, Pb and Zn in soils and sediments. Environ. Geol. 45, 79–85.
Wenzl, T., Haedrich, J., Schaechtele, A., Robouch, P., Stroka, J. (Eds.), 2016. Guidance Document on the Estimation of LOD and LOQ for Measurements in the Field of Contaminants in Feed and Food, p. 52.
Whiticar, M.J., 1996. Stable isotope geochemistry of coals, humic kerogens and related natural gases. Int. J. Coal Geol. 32, 191–215, 1-4.
WHO - World Health Organization, 2021. Global Air Quality Guidelines. Particulate Matter (PM2.5 and PM10), Ozone, Nitrogen Dioxide, Sulfur Dioxide and Carbon Monoxide. World Health Organization, p. 273.
Widory, D., 2007. Nitrogen isotopes: tracers of origin and processes affecting PM10 in the atmosphere of Paris. Atmos. Environ. 41, 2382–2390.
Widory, D., Roy, S., Le Moullec, Y., Goupil, G., Cocherie, A., Guerrot, C., 2004a. The origin of atmospheric particles in Paris: a view through carbon and lead isotopes. Atmos. Environ. 38, 953–961.
Widory, D., Fiani, E., Le Moullec, Y., Gruson, S., Gayrard, O., 2004b. Développement d'une méthode de caractérisation des contributions des sources fixes aux émissions atmosphériques de particules utilisant le traçage multi-isotopique. Application au cas de l'agglomération parisienne. (Doctoral dissertation in French), p. 115, 54 figures, 19 tableaux. BRGM/RP-53335-FR.
Yeh, H.C., Muggenburg, B.A., Harkema, J.R., 1997. In vivo deposition of inhaled ultrafine particles in the respiratory tract of rhesus monkeys. Aerosol Sci. Technol. 27, 465–70.
Yuill, R.S., 1971. The standard deviational ellipse; an updated tool for spatial description. Geogr. Ann. Ser. B Hum. Geogr. 53 (1), 28–39.